ELSEVIER

Contents lists available at ScienceDirect

# **Building and Environment**

journal homepage: www.elsevier.com/locate/buildenv





# Influence of data pre-processing and sensor dynamics on grey-box models for space-heating: Analysis using field measurements

Xingji Yu<sup>a,\*</sup>, Kristian Stenerud Skeie<sup>b</sup>, Michael Dahl Knudsen<sup>c</sup>, Zhengru Ren<sup>d</sup>, Lars Imsland<sup>e</sup>, Laurent Georges<sup>a</sup>

- <sup>a</sup> Department of Energy and Process Engineering, Faculty of Engineering, NTNU Norwegian University of Science and Technology, Kolbjørn Hejes vei 1a, 7034, Trondheim. Norway
- b Department of Architecture and Technology, Faculty of Architecture and Design, NTNU -Norwegian University of Science and Technology, Alfred Getz' vei 1, 7034,
  Transleim Norway
- <sup>c</sup> Department of Civil and Architectural Engineering, Aarhus University, Inge Lehmanns Gade 10, 8000, Aarhus C, Denmark
- d Department of Marine Technology, Marinteknisk senter, NTNU Norwegian University of Science and Technology, Tyholt Otto Nielsens veg 10, 7052, Trondheim, Norway
- <sup>e</sup> Department of Engineering Cybernetics, Faculty of Information Technology and Electrical Engineering, NTNU Norwegian University of Science and Technology, O. S. Bragstads plass 2, 7034, Trondheim, Norway

#### ARTICLE INFO

# Keywords: Data pre-processing Grey-box modeling Building thermal mass Model identifiability Sensor measurement

#### ABSTRACT

A grey-box model is a combination of data-driven and physics-based approaches to modeling. For applications in buildings, grey-box models can be used as the control model in model predictive control (MPC) or to characterize the thermal properties of buildings. In a previous study using data generated from virtual experiments, the influence of data pre-treatment on the performance of grey-box models has been demonstrated. However, field measurement differs from data generated using building performance simulation (BPS). This is because the precision and accuracy, the location, and the dynamics of the sensors could be different. Consequently, this paper extends previous results and conclusions using a real test case of a highly-insulated residential building. The results confirm that data pre-processing has a minimal influence on the identified results (parameter values and simulation performance) for deterministic models. On the contrary, data pre-treatment influences the performance of stochastic models as follows. Firstly, large sampling time  $(T_s)$  can cause the parameters to become nonphysical and can sometimes reduce the one-day ahead prediction performance. With large Ts, the anti-causal shift (ACS) proves to be beneficial to keep the parameters physically plausible while low-pass filtering can also contribute but to a lesser extent. With large Ts, ACS does not guarantee a higher one-day ahead prediction performance for stochastic models, whereas pre-filtering generally has a positive impact. Secondly, for the stochastic model, the sensor dynamics should be modeled if the sensor has a noticeable time constant to guarantee the physical plausibility of the parameters. Thirdly, the dynamics of the hydronic radiator do not need to be modeled if the time constant in the temperature sensors is larger than the radiator. These findings provide practical guidelines for grey-box modeling of buildings with field measurement data.

## 1. Introduction

The mathematical modeling of the thermal dynamics of a building is typically divided into three main categories [1]: white -, black-, and grey-box models. White-box models are based on physical laws (e.g. mass-, energy- and momentum balance equations). The white-box models are generally mathematically complex but have high accuracy. Black-box models are pure data-driven methods based on the measured

time-series data from the system. This method needs sufficient training data to guarantee the accuracy of the model [2]. Grey-box modeling is a combination of these two techniques. This method takes the dominant physical processes to construct the model structure of the system and then fits the model parameters with the measurement data. Lumped resistance and capacitance models are used (i.e. RC models) to construct the grey-box model structure of a building, which means the thermal dynamics of the building are expressed by an electric circuit analogy [3, 4]. Grey-box models are said to have better extrapolation properties

E-mail address: xingji.yu@ntnu.no (X. Yu).

<sup>\*</sup> Corresponding author.

#### Nomenclature

RES Renewable Energy Sources

DR Demand Response

MPC Model Predictive Control

BPS Building Performance Simulation RC Resistance and Capacitance

SNR Signal to Noise Ratio PRBS Pseudo-Random Binary Signal

PI Proportional Integral

NRMSE Normalized Root Mean Squared Error

MBE Mean Bias Error

PSO Particle Swarm Optimization

ACS Anti-Causal Shift
DS Direct Sampling
MA Moving Average
FIR Finite Impulse Response
Det Deterministic Model
Sto Stochastic Model

HTC Heat Transfer Coefficient

HC Heat Capacitance

than black-box models [5]. In addition, they have been widely applied to solve problems in building technologies, such as building load estimation, control and optimization, and building-grid integration [6,7]. The paper focuses on two main applications of grey-box models which are model predictive control (MPC) and characterization of the thermal properties of buildings using field measurements [6,8].

- 1. The emergence of MPC in buildings is related to the concept of energy flexibility and demand response (DR). The conventional electric energy system is undergoing dramatic changes due to the steadily rising share of renewable energy sources (RES). Power generation from RES is often decentralized and intermittent, which may cause considerable volatility to the electric grid. The power imbalance in the supply and demand sides can have severe implications for power quality and reliability [9]. Therefore, more flexible resources are needed to enable increasing penetration of intermittent RES. Demand response (DR) is gaining more attention in power system operations recently, driven by the smart grid concept [10]. Demand response means changes in energy use by the end-use customer from their normal consumption patterns in response to a specific penalty signal (e.g. price signal, CO<sub>2</sub> intensity factor for electricity signal) [10-13]. DR is closely related to the concept of energy flexibility defined by the IEA EBC Annex 67 as the ability of a building to manage its demand and generation according to local climate conditions, user needs and grid requirements [14]. Model predictive control (MPC) is considered a suitable technique for performing DR in a building [7,15] or for activating building energy flexibility [14]. Regarding space-heating, the thermal mass of a building can be a significant short-term heat storage to perform DR [16-20]. The exploitation of such thermal storage requires the indoor temperature  $% \left( 1\right) =\left( 1\right) \left( 1\right$ to fluctuate within limits that are acceptable for the occupants. Previous studies have identified significant DR potential in using economic model predictive control (E-MPC) to exploit the thermal mass of residential buildings, see e.g. Refs. [21-23]. In these applications, grey-box models should enable adequate prediction to achieve good control performance.
- 2. Developing a suitable grey-box model with physically plausible (interpretable) parameters is appreciated from the building analysis point of view [19]. Physically reasonable parameters in grey-box models could contribute to characterizing the thermal properties of

a building using field experiments, such as the overall heat transfer coefficient (HTC).

Data can be processed (or altered) by sensors, the data acquisition system (DAQ) or by the modeler before being used for model identification. Data pre-processing (or data pre-treatment) is acknowledged to have a key influence on the model identification results [24]. For instance, Ljung et al. [25] have analyzed this theoretically and demonstrated the strong influence of the sampling time. However, this topic has hardly been addressed in the specific field of grey-box models for building thermal dynamics. One exception is Madsen et al. [8] that mentioned the importance of data pre-processing in their guidelines, but they did not discuss the topic in detail in their report. Therefore, the main objective of the paper is to systematically investigate the influence of different data pre-processing techniques on the performance of grey-box models for the building thermal dynamics, with MPC and the physical plausibility of parameters in focus. In the past, this effect has been studied in Yu et al. [26] with deterministic and stochastic models. However, they used data generated by virtual experiments, namely multi-zone simulations using the building performance simulation (BPS) software IDA ICE [27]. The data pre-processing methods applied in this study are the sampling time, low-pass filtering and the anti-causal shift (ACS) [25]. ACS corresponds to a shift of the input data one step ahead (also equivalent to a backward shift of the output). Several main conclusions have been demonstrated in this previous study [26]:

- For deterministic models, the data pre-processing has limited influence on the identification results. However, the values of the parameters are strongly dependent on the training dataset and can sometimes be physically non-plausible.
- ullet For stochastic models, the parameters are less dependent than the deterministic models on the training dataset. However, they become non-physical without ACS for large sampling time ( $T_s > 15$  min). Large  $T_s$  does not alter the simulation performance of the stochastic model. ACS proved to be extremely beneficial to guarantee the physical plausibility of parameters with large  $T_s$ . Nevertheless, it generally has a negative influence on the simulation performance of the model.

As these important conclusions are based on virtual experiments, the first objective of the paper is to compare these conconclusions to a real test case based on field measurements. Field measurements deviate from virtual experiments in the following way:

- In reality, sensors have finite precision and accuracy, while the temperature and power data exported from BPS is perfect (i.e., noisefree observations).
- In most BPS software, the air volume of each room is supposed to be isothermal. In reality, the temperature field in a room is not uniform. Two important effects should be considered. Firstly, the room air can present significant temperature stratification, especially when the heat emitter is close to maximum power. Secondly, the sensors are usually mounted on a wall in a casing. For sudden changes in the indoor temperature, the measured value with a wall-mounted sensor may thus differ from the real air temperature. The thermal dynamics of the sensor due to the casing can also be seen as a form of implicit data pre-treatment if the sensor dynamics are not modeled.

This paper uses measurement data from an experimental building, the ZEB Living Lab [28,29] to compare the conclusions that were originally based on virtual experiments [26]. Three complete datasets of the indoor temperature corresponding to different sensor locations are available:

 Several temperature sensors without casing are mounted at different heights on a vertical bar located in the middle of different rooms. The averaging of these measurements gives an approximation of the volume-averaged indoor air temperature, which is a good representation of the indoor air temperature  $T_i$  of a mono-zone model (i.e. one zone for the entire building). In addition, the volume-average indoor temperature is less sensitive to the vertical temperature stratification than the measurement from a single sensor.

• For market penetration, it is better to limit the number of temperature sensors to one in each room. Thus, it is important to investigate the possibility of identifying a proper grey-box model with measurements from a single temperature sensor. Firstly, one temperature sensor is located on a vertical bar at a medium height in the living room. The stratification effect at mid-height should be lower than the top and low locations in the room. Secondly and probably the most realistic configuration, another temperature sensor is mounted on a wall at the same mid-height location as the previous sensor (placed on the bar).

The second objective of the paper is to analyze how the type of indoor temperature measurement influences the performance of the greybox models.

The main objective is to identify the specific influence of different data pre-processing techniques on the grey-box model performance. Other phenomena that could have an impact on the model performance, such as overfitting, should be removed from the analysis. Therefore, model structure selection is performed in detail in this paper before starting to analyze the influence of the data pre-treatment. It starts with a review of the literature regarding the structure of grey-box models. This results in the selection of a set of structures to be evaluated. The evaluation includes the analysis of structural and practical identifiability of the selected models, their prediction performance and physical plausibility of the parameters. Checking structural identifiability is the prerequisite in the model identification process [30,31]. This property guarantees that the parameters can be uniquely determined from the input-output data under ideal conditions of noise-free observations and error-free model structure. The structural identifiability of the candidate models in this study is verified using DAISY software [30]. However, field measurement data always contain noise and error, which challenges the practical identifiability of the model. Therefore, the prediction performance and the physical plausibility of parameters are taken as the criteria for the model selection. Finally, for stochastic models, a cumulative periodogram is used as an additional criterion to prove that the model is complex enough to capture the building dynamics.

The remainder of the paper is structured as follows. Section 2 provides information on the experimental setup, which includes the building geometry, measurement devices, the definition of test cases and the boundary conditions. Section 3 describes the methodology of this study, including the grey-box model structure and data pre-processing techniques used for this study. The algorithm to identify the grey-box model parameters is also outlined, followed by the definition of key performance indicators (KPIs). Section 4 gives the results and is divided into three main aspects. The most suitable model structure is selected with the original data with 5 min sampling time and the volume-averaged temperature. Then, the influence of data pre-processing and the sensor selection is presented. Finally, conclusions are presented in Section 5.

#### 2. Description of experiments

# 2.1. Case building

The experiments performed in this study were carried out in the ZEB Living Lab, a single-family, zero-emission house with a heated floor area of about  $100 \text{ m}^2$  on the campus of the Norwegian University of Science and Technology (NTNU) in Trondheim. The building envelope has a wooden frame with mineral wool measuring 35–40 cm and a glazing ratio of 0.2. The space-heating can be floor heating, a central radiator, or

ventilation air. The ventilation system is equipped with a heat recovery unit. By operating the doors in the building, four zones can be created (bedroom west, bedroom east, bathroom, and living areas). The appearance of the building and the internal layout of the Living Lab is shown in Fig. 1. This study is based on two sets of experiments in this building with different space-heating emission systems and different periods of the space-heating season. Data from using two different heat emitters are used to make the conclusions more general.

The first set of experiments (from the 18th April to 15th May 2017) used an electric heater for space-heating. Detailed information on the measurement setup and data can be found in previous work [28,32]. The corresponding length of these three experiments are 6 days, 11 days and 7 days, respectively. The electric heater of 2.6 kW was placed in the center of the building (the heater is marked in red in Fig. 1 (b)). A pseudo-random binary signal (PRBS) has been applied to the electric heater to excite the thermal dynamics of the building. PRBS is a periodic and deterministic signal with white noise properties and a high signal-to-noise ratio (SNR). The PRBS signal activates the dynamic system at a broad range of frequencies.

Four experiments were carried out, and only the last three were successful. The successful experiments are named Experiments 2, 3, and 4 (i.e., Experiment 1 was discarded). The dataset has a time interval of 5 min. The measurements include the outdoor temperature, indoor air temperatures, global solar irradiation and electricity consumption, including the radiator power (Qh). To avoid modeling the air-handling unit (AHU), the ventilation losses from the mechanical ventilation are introduced as one input to the grey-box model in this study. These ventilation losses are explicitly pre-calculated with the measured temperature difference between the supply and exhaust ventilation air combined with the measured airflow rate (constant air volume, CAV). The electric heating system has negligible thermal inertia compared to the building envelope, so it is assumed that the dynamics of the radiators play a limited role. Experiments 2 and 4 were conducted with internal doors opened, which theoretically should lead to a more uniform spatial distribution of the air temperature inside the building while all the doors were closed in Experiment 3. Air was pre-heated using a heating coil in Experiment 4 only. The building is unoccupied in all the experiments, but electric dummies operated by a control schedule have been used leading to realistic internal gains.

# 2.2. Experiment with the hydronic radiator

The experiment with the hydronic radiator was initially performed to investigate cost-effective MPC implementation (E-MPC) with control of the hydronic radiator in a Norwegian zero-emission building (Living Lab) [29]. The experiment lasted for approximately one month (from mid February to mid March 2017), with an 18-day excitation phase and an E-MPC operation phase of two weeks. A randomly generated binary signal switching the radiator temperature set-point between 21  $^{\circ}\text{C}$  and 24  $^{\circ}\text{C}$  was created to excite the thermal dynamics of the building and collect measurements for training the model. This new training dataset is based on six days in February and is named here as Experiment 5. The dataset has a time interval of 5 min.

The hydronic radiator has a rated power of 4.7 kW (at rated temperature 75 °C/65 °C) and was in the same place as the electric heater. The supply water temperature was maintained at about 55 °C leading to a maximum radiator power of 2.5 kW. The thermostatic valve in the radiator adjusts the mass flow using a proportional-integral (PI) controller to track the set-point temperature. Compared to the electric heater, the thermal mass of the hydronic radiator with 113 kg of steel cannot be neglected. The power delivered to the hydronic radiator ( $Q_h$ ) is measured by an energy meter based on the difference between supply and return temperatures. When the hydronic radiator is switched on, the initial water temperature in the radiator is close to the indoor air temperature. Due to the thermal mass of the radiator, it takes time for the return temperature to heat up and reach steady-state (when the power

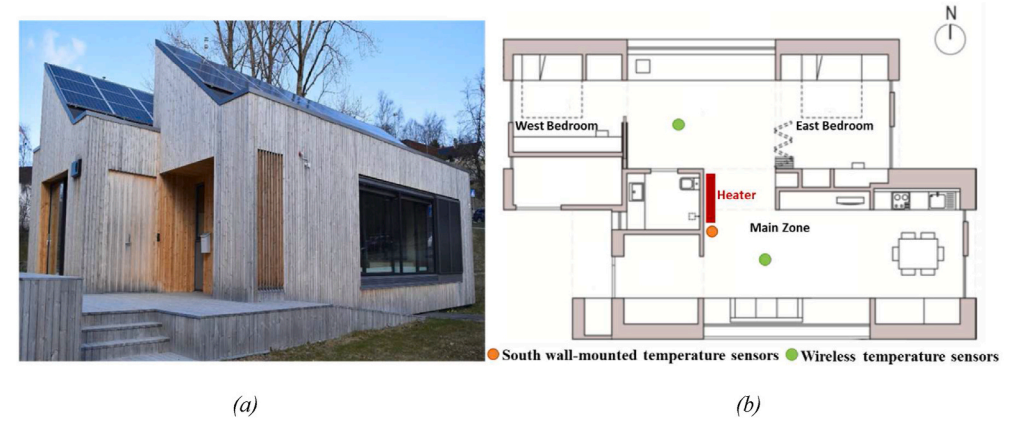


Fig. 1. View of the ZEB Living Lab (a) and floor plan of the ZEB Living Lab with temperature sensor location (b).

delivered to and emitted by the radiator are equal). This makes a large difference in supply and return temperatures at the beginning, leading to a very high start-up peak for  $Q_h$ . The maximum emitted power of the radiator in steady-state is around 2.5 kW, while the maximum delivered power during start-up periods is around 4.0 kW. This confirms that the thermal dynamics of the hydronic radiator are significant. The summary of all the experiments used in this study is given in Table 1.

#### 2.3. Indoor temperature measurement

In the experiments with the electric heater, PT100 sensors with an accuracy of  $\pm 0.1$  K are placed at different locations in the building; see details in Ref. [28]. This leads to the definition of three datasets:

- Two available datasets correspond to different placement of PT100 temperature sensors without casing and with wireless transmitters. They are placed in a vertical bar in the middle of the two living rooms (see green dots in Fig. 1 (b) and Fig. 2 (a)). For each bar, the height of the six sensors is 0.18 m, 0.95 m, 1.6 m, 1.7 m, 2.3 m and 3.4 m, respectively. The *volume-averaged temperature* of the building is calculated using the measurement from all the sensors placed in the vertical bars and evaluated using the volume average at each horizontal layer. The *single sensor without casing* dataset corresponds to the measurement at 1.6 m in the living room south. The height of 1.6 m is close to the middle height of the building, where the influence of stratification is expected to be minimal (meaning that the measured temperature at 1.6 m is the closest to the volume-averaged temperature).
- The third dataset is based on PT100 sensors mounted on the wall in a casing (see the orange dot in Fig. 1 (b) and Fig. 2 (b)). The height of the wall-mounted sensors is 0.1 m, 0.8 m, 1.6 m, 2.4 m and 3.2 m, respectively. The third dataset corresponds to the measurement of a *single wall-mounted sensor* mounted in the south of the living room at the height of 1.6 m.

In the experiments with the hydronic radiator, only the temperature measurements from the wall-mounted temperature sensor are available.

Fig. 3 shows the temperature reading from the wireless temperature sensors with different heights (0.18 m, 1.6 m and 3.4 m) and the wall-

mounted temperature sensor (1.6 m) against the volume-averaged temperature. The stratification of the temperature of the wireless temperature sensors at different heights can be observed. The stratification gets larger when the solar radiation or the radiator power is large. The reason for choosing the sensor in the south was to capture the influence of solar radiation. The thermal dynamics of the wall-mounted sensor can also be observed. The reading from the wall-mounted sensor is smoother compared to the volume-averaged temperature and the readings from the single wireless temperature sensors.

#### 3. Methodology

#### 3.1. Grey-box model structure

The structure of the grey-box models is derived from the conservation of energy. The physics modeled by the grey-box models is the heat transfer between the building and its outdoor environment, the solar radiation and internal gains.

The ZEB Living Lab is super-insulated with an efficient heat recovery of the ventilation air. These two points lead to limited temperature differences between rooms [33] (compared to the temperature difference between indoor and outdoor air) even if internal doors are closed. Consequently, the building can be modeled as one thermal zone (i.e., the mono-zone model with a unique node to represent the indoor temperature). Previous studies [29,32,34] confirmed that a mono-zone greybox model is able to make an accurate prediction on the air temperature in the ZEB Living Lab, for closed and open internal doors.

Grey-box modeling is a very common approach and a considerable amount of research has already been applied to this method. In their study, Viot et al. [35] provided a comprehensive list of research papers on MPC that used RC models. Bacher and Madsen [36] identified a suitable model using data obtained from an unoccupied office building. The probability ratio tests were used to analyze models of different orders. The results showed that increasing the model order from the third-order does not substantially improve the results. In Ref. [37], Berthou et al. found that the second-order model performs best for occupied office buildings. Braun et al. [38], Hu et al. [39] and Goyal [40] used the second-order model as the base component for the multi-zone model of the building. It was concluded that the

Table 1
Summary of the four experiments, "Full set" means all measurements of volume-averaged, single sensor (no casing), wall-mounted sensor are available.

Experiments	Radiator	Door	Sampling time	Period	Use	Temperature Sensor
2	Electric	Open	5 min	18/04-24/04 (2017)	Validation	Full set
3	Electric	Closed	5 min	27/04-08/05 (2017)	Validation	Full set
4	Electric + AHU	Open	5 min	08/05-15/05 (2017)	Training	Full set
5	Hydronic	Open	5 min	22/02–27/02 (2019)	Training	Wall-mounted

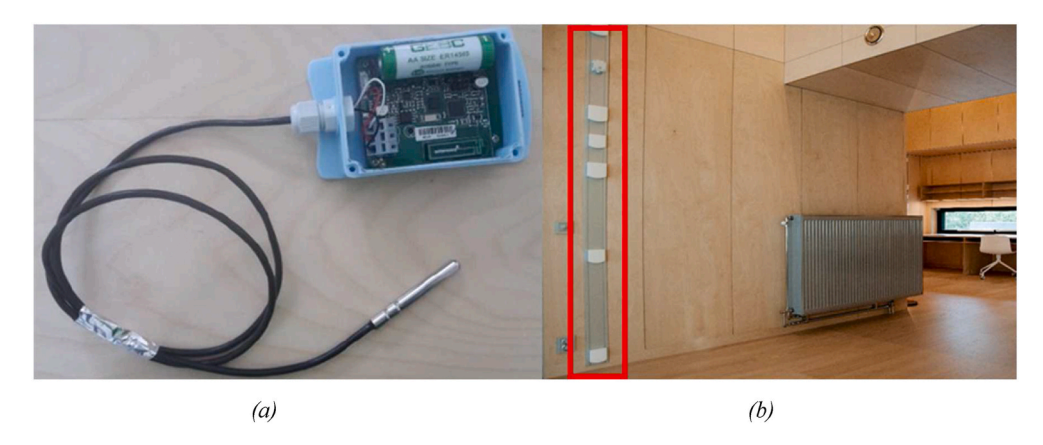


Fig. 2. Wireless temperature sensors (a) and wall-mounted temperature sensors (b).

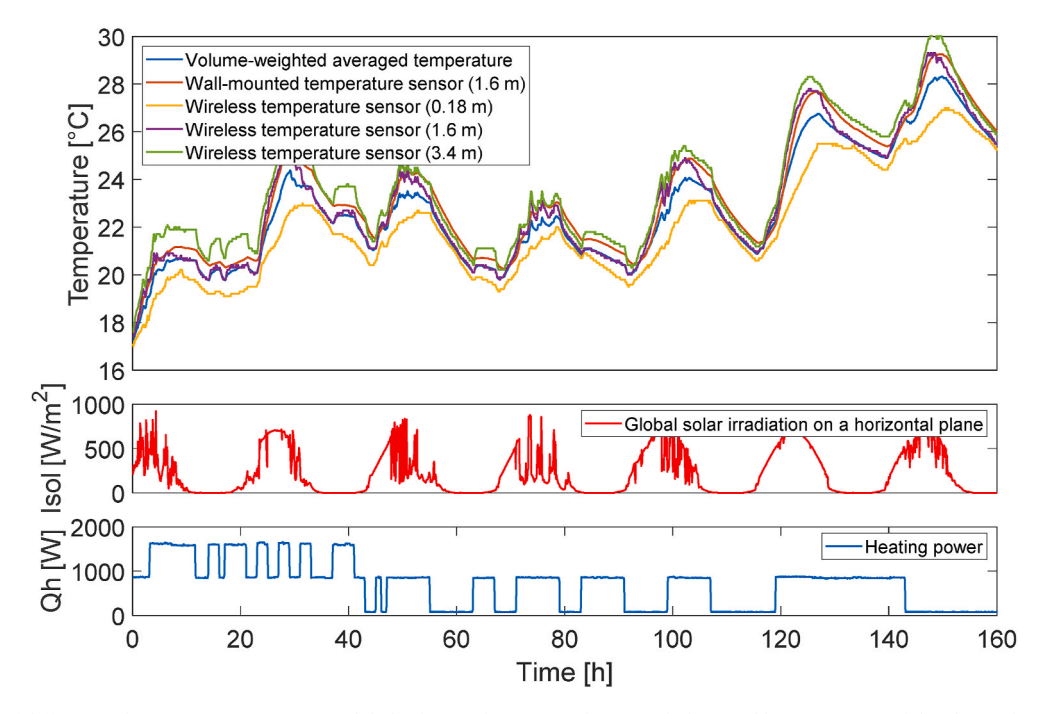


Fig. 3. Comparison of different indoor temperature sensors, global solar irradiation on a horizontal plane and heating power of the electric heater for Experiment 4.

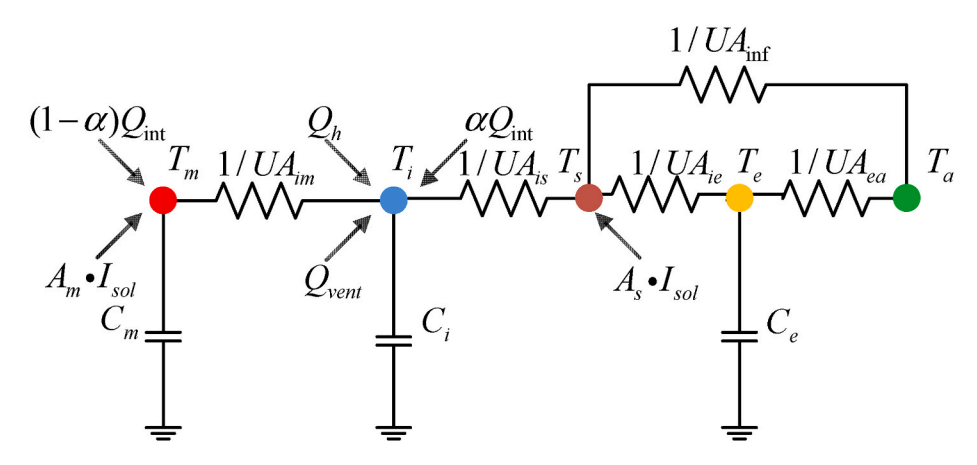


Fig. 4. Structure of the 5R3C model.

second-order model is sufficient for good prediction results for indoor temperature and heating power by Palomo Del Barrio et al. [41] and Reynders et al. [42]. Brastein et al. [43] showed that deterministic grey-box models at second-order could face the problem of practical identifiability. Yu et al. [34] proposed two grey-box model structures derived from VDI 6007 [44] and ISO 13790 [45]. The results were that with few measurements and a large number of unknown parameters, the identified parameters could easily become non-identifiable. Furthermore, due to overfitting and convergence issues, Reynders et al. [42] concluded that heat flux measurements were needed to ensure observability for higher-order models (i.e. fourth- and fifth-order models). Thus, based on these previous studies, our paper only considers the model structure up to the third-order.

As a result, seven mono-zone model structures limited to third-order have been taken from the existing literature [36,42,46]. The selection process will determine the best model structure to be used to investigate the specific influence of data pre-processing. These seven models correspond to different combinations of RC components and splitting factors for the distribution of internal gains between the nodes. According to report [28], some sensors in the ZEB Living Lab at specific locations were directly exposed to solar radiation at certain periods of the day, which makes some of the measurements an unsatisfactory representation of the air temperature. The dataset in Experiment 4 with open internal doors is chosen as the training dataset for the case with the electric heater. Only the 5 min dataset is used for the model selection to avoid aliasing errors. The datasets in Experiments 2 and 3 were used as the validation datasets to analyze the prediction performance of the models. Structural identifiability is a prerequisite for system identification [47], which refers to the theoretical possibility of determining the parameter values from the input and output data. Thus, the structural identifiability of the candidate model structures has been tested by the DAISY software [30,48] before implementing the identification process. The result is that all the seven grey-box model structures are structurally identifiable. The most complex structure is the 5R3C model and is shown in Fig. 4. Other model structures are obtained by simplification and can be found in the Appendix. The physical meaning of the model parameters is listed in Table 2.

The corresponding state-space model of Fig. 4 is given by:

 Table 2

 The physical interpretation of the parameters of all grey-box models.

Parameters	Physical interpretation and unit
$T_i$	Temperature of the internal node (i.e., indoor air, furniture) [°C].
$T_e$	Temperature of the external walls [°C].
$T_s$	Temperature of the internal wall surfaces of external walls [°C].
$T_m$	Temperature of the internal walls [°C].
$T_a$	The outdoor (or outdoor) temperature [°C].
$C_i$	Heat capacity including the thermal mass of the air, the furniture [kWh/K].
$C_e$	Heat capacity of the node external wall for the second-order and third- order models [kWh/K].
$C_m$	Heat capacity of the node internal wall for the third-order model [kWh/K].
UA	Overall heat transfer coefficient (HTC) between T <sub>i</sub> and T <sub>a</sub> [kW/K].
$UA_{ie}$	Heat conductance between the building envelope and the interior [kW/K].
$UA_{ea}$	Heat conductance between the outdoor and the building envelope [kW/K].
UA <sub>inf</sub>	Heat conductance between the outddoor and the interior node (components with negligible thermal mass, like windows and doors) [kW/K].
$UA_{im}$	Heat resistance between the internal thermal mass and the interior node [kW/K].
$UA_{is}$	Heat resistance between the indoor wall surface and the interior node [kW/K].
$Q_{int}$	Internal heat gain from artificial lighting, people and electric appliances [kW].
$Q_h$	Heat gain delivered to the heat emitter [kW].
$Q_{vent}$	Heat gain from the ventilation (pre-computed using measurements) [kW].
$I_{sol}$	Global solar irradiation on a horizontal plane [W/m <sup>2</sup> ].
$A_i$	The effective window area of the building corresponding to T <sub>i</sub> [m <sup>2</sup> ].
$A_e$	The effective window area of the building corresponding to $T_{\rm e}\ [{\rm m}^2]$ .
$A_m$	The effective window area of the building corresponding to $T_m$ [ $m^2$ ].
$A_s$	The effective window area of the building corresponding to $T_s$ [m <sup>2</sup> ].
$\alpha$	Fraction of internal gains injected to the internal node.

#### 3.2. Model identification tool and optimization

Both the deterministic and stochastic models are investigated using the MATLAB system identification toolbox [49]. The stochastic models are formulated as an extension of deterministic models (K=0) [8]. The generic equations of the stochastic linear state-space model in innova-

(4)

$$\begin{bmatrix} T_{e}(t) \\ T_{i}(t) \\ T_{m}(t) \end{bmatrix} = \begin{bmatrix} \frac{(UA_{ie} + UA_{ea})}{C_{e}} + \frac{UA_{ie}^{2}}{C_{e} \cdot (UA_{is} + UA_{ie} + UA_{inf})} & \frac{UA_{ie} \cdot UA_{is}}{C_{e} \cdot (UA_{is} + UA_{ie} + UA_{inf})} & 0 \\ \frac{UA_{ie} \cdot UA_{is}}{C_{i} \cdot (UA_{is} + UA_{ie} + UA_{inf})} & -\frac{(UA_{im} + UA_{is})}{C_{i} \cdot (UA_{is} + UA_{ie} + UA_{inf})} & \frac{UA_{im}}{C_{i}} \\ 0 & \frac{UA_{im}}{C_{m}} & -\frac{UA_{im}}{C_{m}} \end{bmatrix} \begin{bmatrix} T_{e}(t) \\ T_{i}(t) \\ T_{m}(t) \end{bmatrix}$$

$$+ \begin{bmatrix} \frac{UA_{ea}}{C_{e}} + \frac{UA_{ie} \cdot UA_{inf}}{C_{e} \cdot (UA_{is} + UA_{ie} + UA_{inf})} & \frac{UA_{ie} \cdot UA_{inf}}{C_{e} \cdot (UA_{is} + UA_{ie} + UA_{inf})} & 0 & 0 & 0 \\ \frac{UA_{is} \cdot UA_{ie}}{C_{e} \cdot (UA_{is} + UA_{ie} + UA_{inf})} & \frac{UA_{ie} \cdot UA_{inf}}{C_{e} \cdot (UA_{is} + UA_{ie} + UA_{inf})} & \frac{\alpha}{C_{i}} & \frac{\alpha}{C_{i}} & \frac{1}{C_{i}} \\ \frac{UA_{is} \cdot UA_{ie}}{C_{i} \cdot (UA_{is} + UA_{ie} + UA_{inf})} & \frac{UA_{is} \cdot A_{s}}{C_{i} \cdot (UA_{is} + UA_{ie} + UA_{inf})} & \frac{\alpha}{C_{i}} & \frac{\alpha}{C_{i}} & \frac{1}{C_{i}} \\ 0 & \frac{A_{m}}{C_{m}} & \frac{1-\alpha}{C_{m}} & \frac{1-\alpha}{C_{m}} & 0 \end{bmatrix} \begin{bmatrix} T_{a}(t) \\ U_{ont}(t) \\ U_{oven}(t) \\ U_{oven}(t) \\ U_{o}(t) \end{bmatrix}$$

$$(1)$$

tive form are expressed as:

y(t) = Cx(t) + e(t)

$$y(t) = \begin{bmatrix} 0 & 1 & 0 \end{bmatrix} \begin{bmatrix} T_e(t) \\ T_i(t) \\ T_m(t) \end{bmatrix}$$

$$(2) \qquad \frac{dx}{dt} = Ax(t) + Bu(t) + Ke(t)$$

$$(3)$$

where x is the state vector, A, B and C are the system matrices, u is the input vector (i.e.  $T_a$ ,  $I_{sol}$ ,  $Q_{int}$ ,  $Q_h$ ) and y is the output (i.e. indoor temperature,  $T_i$ ). K is the disturbance matrix of the innovation form (Kalman gain) [50]. The matrices A, B, C and K are functions of the model parameters ( $\theta$ ). The continuous-time model is discretized to identify the model parameters using discrete-time series measurement. The time discretization in the MATLAB system identification toolbox assumes piecewise-constant input data during each time interval (i.e. zero-order hold).

Yu et al. [26] proved that the global optimization routine is more likely to avoid the local optimum compared to the pure gradient-based optimization routine. Wang et al. [51] successfully used the swarm-based optimization algorithm to estimate the parameters of thermal dynamic models. Thus, this paper also takes the global optimization routine to identify the parameters. The global optimization routine resorts to the heuristic particle swarm optimization (PSO) at the first stage. Then the default gradient-based optimization function (greyest) in the MATLAB identification toolbox is applied in the second stage to further polish the results. The objective function f(x) of the optimization is defined as Equation (5).

$$f(x) = \sqrt{\frac{\sum_{k=1}^{N} ||y_k - \hat{y_k}(\theta)||^2}{N}}$$
 (5)

where  $y_k$  is the measurement output, while  $\widehat{y}_k(\theta)$  is the prediction of the model (i.e., a simulation for the deterministic model and one-step ahead prediction for the stochastic model).

#### 3.3. Data pre-processing techniques

Three distinct data pre-treatments are investigated in the paper. They are sampling, low-pass filtering and anti-causal shift (ACS). The original dataset has a sampling time ( $T_s$ ) of 5 min which is faster than the highest frequency of the input signal ( $T_{min}$ ), such as the PRBS signal. Ljung et al. [25] demonstrated that longer sampling time with  $T_s > T_{min}$  can lead to non-physical value and variance for the identified parameters, as confirmed by Yu et al. [26] in the context of the thermal dynamics of the building. To investigate this effect, sampling times of increasing duration are considered in our investigations, namely 15, 30 and 60 min. Before resampling the data, a low-pass filter can be applied. This leads to three scenarios:

- Direct sampling (DS): Sampling at T<sub>s</sub> without pre-filtering, which may cause large aliasing errors for large T<sub>s</sub>.
- Moving-average (MA) filter: The original 5 min data is averaged over a
  period T<sub>s</sub> in the past before sampling. This can significantly decrease
  the aliasing error and it also conserves the integral of the physical
  quantity, such as energy.
- Finite impulse response (FIR) filter: A FIR with a cut-off frequency of 1/ T<sub>s</sub> is applied before sampling. The frequency content higher than the cut-off frequency is removed, which leads to a negligible aliasing error (if the FIR is designed at a sufficient order).

The low-pass filters are applied to all input and output variables in the dataset. Thus, theoretically, no delay will be introduced in the dataset, which could influence the final results. The conclusion would be different if the low-pass filter was applied to a subset of the input and output data.

Finally, time labeling plays a role in aligning inputs and outputs for the identification application [25]. As shown by Ljung et al. [25], a time shift, called anti-causal shift (ACS), of the input (Input Delay =  $-T_s$ ) is beneficial for model identification with large  $T_s$ .

#### 3.4. Dynamics of the wall-mounted sensor

Section 2.4 showed that the wall-mounted sensors have nonnegligible thermal dynamics. Consequently, the grey-box model structures introduced in Section 3.1 should be adapted to account for the effect of the time constant of sensor dynamics and thus avoid potential mistakes in the model identification process. As proposed in Bacher et al. [36], it is possible to add an additional node for the temperature sensor, leading to an extra resistance  $(R_{\text{s}})$  and capacitance  $(C_{\text{s}})$ . However, the authors also pointed out that it was not possible to give a physical interpretation for the value of  $C_{\text{s}}$ . This was also found from our preliminary tests based on our data. Therefore, we rather introduced an adaptation of the model with a single additional parameter, the time constant of the sensor  $\tau=R_{\text{s}}C_{\text{s}}$ . The model decreased the number of parameters compared to the version in the study [36] to increase the identifiability of the model. The dynamics for the sensor node is expressed by the following equation:

$$\frac{dT_{sensor}}{dt} = \frac{1}{\tau} \left( T_i - T_{sensor} \right) \tag{6}$$

where  $T_i$  is the temperature of the internal node,  $T_{sensor}$  is the temperature measurement from the wall-mounted temperature sensors.

# 3.5. Key performance indicator

Several key performance indicators (KPIs) are defined to evaluate the model performance. They can be divided into two categories: the physical plausibility of the identified parameters and the prediction performance of the model.

Physical plausibility means that the calibrated value of the model parameters should give a physically reasonable estimate of the thermal properties of the building. For conciseness in our study, it is not possible to report the value and variance of all the model parameters. However, the key parameters that are enough to support our conclusions will be presented: the overall heat transfer coefficient (HTC) and the capacitances ( $C_i$  and  $C_e$ ). In addition, one parameter modeling the influence of the solar radiation, the effective window area ( $A_i$ ), will also be taken as KPI when the influence of the data pre-processing is discussed.

The overall heat transfer coefficient (HTC) is the total heat loss of the building in steady-state. Heat transfer by convection and long-wave radiative heat transfer is nonlinear. However, heat conduction is dominant and has good linear properties if the building is highly insulated and airtight. The combination of several resistances of the grey-box model forms the HTC, which is defined by Equation (7) for the 3R2C model.

$$HTC = \frac{1}{1/UA_{ie} + 1/UA_{ea}} + UA_{inf}$$
 (7)

Therefore, only the value of the HTC is shown in the later discussion, not its variance. Clau $\beta$  et al. [52] evaluated the HTC value of the ZEB Living Lab to be 83 W/K, which is used as the reference value for the HTC in this work.

It is challenging to define a physically plausible range for the capacitances ( $C_i$  and  $C_e$ ) since their values strongly depend on the excitation signal. However, it is possible to obtain a rough indication of  $C_e$ . According to NS3031 (2016) [53], the effective heat capacitance ( $C_{eff}$ ) of lightweight Norwegian buildings is typically within the range of 3.4–6.5 kWh/K. As the  $C_{eff}$  is based on daily excitations of the thermal mass of a building, it can be related to the thermal capacitance  $C_e$  (at least, up to second-order RC models without a node for internal walls,  $T_m$ ).

The long-term prediction performance is of the utmost importance if the main application of the grey-box model is being employed in an MPC. Equation (8) gives the method of calculating the normalized root mean squared error (NRMSE).

$$NRMSE = \frac{||y_k - \hat{y}_k||}{||y_k - mean(y_k)||}$$
 (8)

The NRMSE fitting, defined in Equation (9), is used to evaluate prediction performance. It translates how well the response of the predicted model matches measurement data. If the fit is 100%, the model perfectly matches the measurement data, whereas a low or negative fit is a model of lower quality. The NRMSE fitting value is calculated based on simulation for the deterministic model and one-day ahead prediction for the stochastic model. In other words, for the stochastic model, the model selection is done using the one-step ahead prediction while the ability to perform MPC is evaluated using a one-day ahead prediction.

$$NRMSE_{fit} = (1 - NRMSE) \times 100\% \tag{9}$$

In addition to the NRMSE fitting value, the mean bias error (MBE) defined by Equation (10) is also used as a complementary index. Theoretically, an MBE value close to zero is best as this means that the residual of the model has a lower mean bias error.

$$MBE = \frac{1}{n} \sum_{k=1}^{n} \left( y_k - \hat{y}_k \right) \tag{10}$$

In practice, the results show that all our models have good MBE properties. Therefore, this index has been used but is not reported in the paper.

#### 4. Results

This section is divided into three parts. Firstly, the selection of the best model structure is presented and discussed. With the best model, the influence of data pre-processing and the type of indoor temperature measurement are then studied. Finally, the results are analyzed for deterministic and stochastic models. Most of the results presented are based on the datasets with the electric heaters (Experiments 2–4). The description of each case presented in this section is given in Table 3.

#### 4.1. Model selection

The results for the electric radiator and the seven models using the volume-averaged temperature and the baseline  $T_s$  of 5 min are summarized in Table 6 in Appendix, while the key results are presented in Table 4.

- The first-order 1R1C model is not enough to describe the heat dynamics of the building for neither the deterministic nor the stochastic models. This is confirmed by the cumulative periodogram of the residuals in supplementary material. The cumulative periodogram falls largely outside the confidence interval, which indicates poor white noise properties of the residuals.
- The second-order models, 2R2C and 3R2C, show significant improvement in the NRMSE fitting compared to the first-order 1R1C model. The cumulative periodogram of the residuals also stays strictly within the confidence interval.

 Although the third-order models (3R3C to 5R3C) sometimes present better NRMSE fitting with the deterministic model, the identified parameters are not physically plausible for the stochastic model. The capacitance of the interior node C<sub>i</sub> has a larger value than the value of the internal walls node C<sub>m</sub>, which does not translate the actual physics. Furthermore, for the 4R3C and 5R3C stochastic models, the UAea value is identified close to 0, which also violates the reality (as external walls are not perfectly insulated). Regarding the cumulative periodogram of the residuals, the 5R3C is outside the confidence interval while the 3R3C and 4R3C models remain within the confidence interval but do not perform better than the second-order models. The variance of the key parameter Ce also shows that the third-order models could lead to large values with deterministic models, which implies that the third-order models may be overfitting. Further, the variance of C<sub>e</sub> for the stochastic model also shows that the component UAinf is necessary to be modeled. Finally, the objective function during the successive PSO iterations is plotted along with the parameter value. The scatter plots for parameters C<sub>e</sub> and Ai for second-order and third-order models can also be found in supplementary material. It is observed from the scatter plots that the optimum are flatter with third-order models, which corresponds to lower practical identifiability of the models. It can be concluded that the third-order models are (or are close to being) overfitted. The fitting of validation NRMSE fitting also confirms that the secondorder model is the best trade-off between model complexity and accuracy.

In conclusion, second-order grey-box models are most suitable for our study as the prediction performance and the physical plausibility are good. In addition, the dominant physical processes are properly modeled as proven by the cumulative periodogram. The second-order models are selected for the study as they are accurate but not overfitted. This guarantees that the conclusions will not be contaminated by overfitting. Among second-order models, the 3R2C model is taken as the baseline case in the remainder of the paper.

# 4.2. Influence of the temperature measurement

The model selection is based on the volume-averaged indoor temperature at 5 min. In the description of experiments, it has been shown that the indoor temperature is dependent on the type of measurement, see Section 2.4. Consequently, Fig. 5 and Fig. 6 compare the identified value of two key indicators (HTC and  $C_{\rm e}$ ) for the different types of temperature measurement, still using a sampling time of 5 min. For the deterministic model, the difference in temperature measurements has a limited influence on the identified model parameters. However, for the stochastic model, the identified HTC value using the baseline 3R2C model and the single wall-mounted temperature sensor is much larger than the reference HTC value. Furthermore, the variance of  $C_{\rm e}$  is also extremely large. Thus, the time constant of the wall-mounted sensor dynamics has a large impact on the stochastic 3R2C model. This conclusion is also confirmed by the cumulative periodogram of the

**Table 3**Description of the datasets and their corresponding abbreviations.

-				
Case	Sensor	Sensor node in model	Dataset	Use
T1Exp2	Volume-averaged temperature (T1)	No	Experiment 2	Validation
T1Exp3	Volume-averaged temperature (T1)	No	Experiment 3	Validation
T1Exp4	Volume-averaged temperature (T1)	No	Experiment 4	Training
T2Exp4	Single temperature sensor in the air (T2)	No	Experiment 4	Training
T3Exp4	Single wall-mounted temperature sensor (T3)	No	Experiment 4	Training
T4Exp4	Single wall-mounted temperature sensor (T4)	Yes (τ)	Experiment 4	Training
T5Exp5	Single wall-mounted temperature sensor (T5)	No	Experiment 5	Training
T6Exp5	Single wall-mounted temperature sensor (T6)	Yes (τ)	Experiment 5	Training

**Table 4**The values and the corresponding variance of C<sub>e</sub>.

Model	C <sub>e</sub> Value [kWh/K]	C <sub>e</sub> Variance [kWh/K]	NRMSE Fitting (simulation)	NRMSE Fitting (validation)	Model	C <sub>e</sub> Value [kWh/K]	C <sub>e</sub> Variance [kWh/K]	NRMSE Fitting (1- step ahead)	NRMSE Fitting (validation)
1R1Cdet	5.62	0.754	72.7%	55.1%	1R1Csto	4.78	0.437	99.0%	65.7%
2R2Cdet	6.11	0.369	93.0%	75.3%	2R2Csto	6.37	1.77	99.2%	79.2%
3R2Cdet	5.28	0.284	93.6%	79.7%	3R2Csto	4.22	0.748	99.2%	81.8%
4R2Cdet	5.40	0.430	93.5%	72.4%	4R2Csto	4.28	0.726	99.2%	81.5%
3R3Cdet	6.08	0.689	95.0%	78.6%	3R3Csto	11.9	3.92	99.2%	71.1%
4R3Cdet	3.94	0.609	95.3%	75.6%	4R3Csto	4.02	0.709	99.2%	82.7%
5R3Cdet	3.99	0.613	95.3%	76.0%	5R3Csto	5.73	0.718	99.2%	79.8%

(For the first-order 1R1C model, Ce does not exist and the value reported in the table is the value of Ci. Bold values inside the table indicates unphysical parameters.)

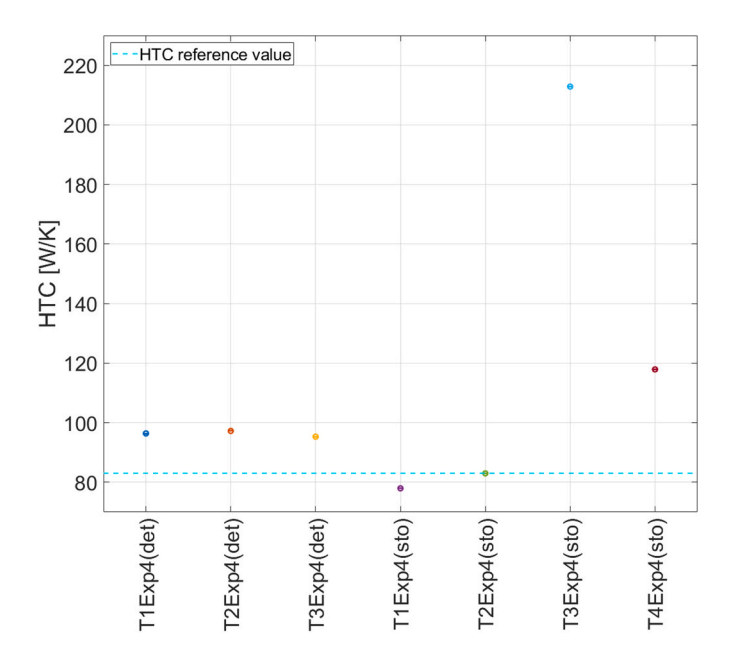


**Fig. 5.** Comparing the HTC of the 3R2C deterministic (det) and stochastic (sto) models using Experiment 4 and different types of temperature measurement (5 min).

residuals in Fig. 7, which shows that the baseline 3R2C model with the wall-mounted sensor does not describe the system dynamics (between  $0.4{\text -}1.4 \times 10^{-3}$  Hz). As introduced in Section 3.4, an adapted model with a time constant for the sensor is added to the original 3R2C model. This adapted model improves the results since the parameters become physically plausible again. In addition, the cumulative periodogram of the residuals confirms this conclusion (see dataset T4Exp4). Furthermore, the one-day ahead prediction comparison in Fig. 8 also shows the significant improvement from the adapted 3R2C compared to the original baseline 3R2C model. The identified time constant ( $\tau$ ) has a value of 8.28 min, thus is larger than the sampling time. For the remainder of the paper, the sensor node will only be analyzed for the stochastic model.

# 4.3. Influence of data pre-processing on grey-box modeling

Until now, the model performance has used a sampling time of 5 min without data pre-processing, which is faster than the Nyquist sampling frequency. The signal is sampled faster than the system dynamics so that it is guaranteed that it does not influence the results. Consequently, the specific influence of data-preprocessing can be identified in the present section. The analysis of deterministic and stochastic models should be clearly distinguished.

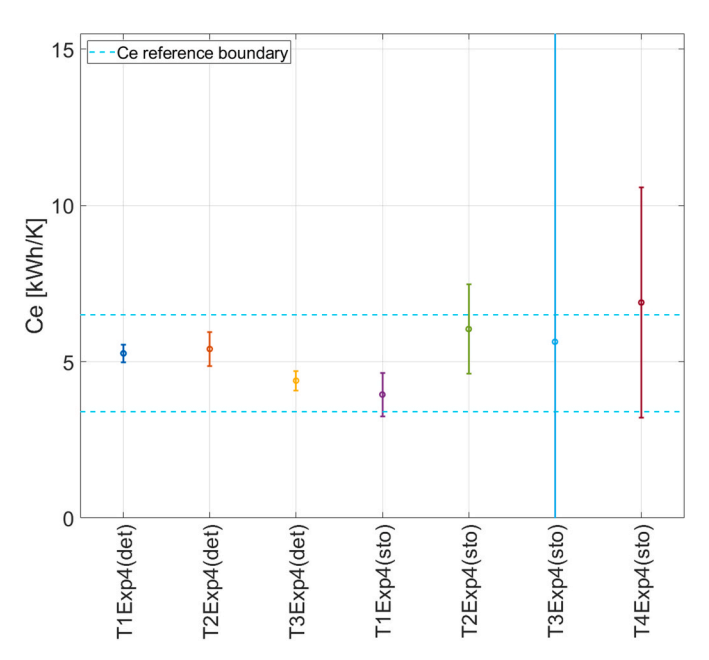


**Fig. 6.** Comparing the Ce of the 3R2C deterministic (det) and stochastic (sto) models using Experiment 4 and different types of temperature measurement (5 min).

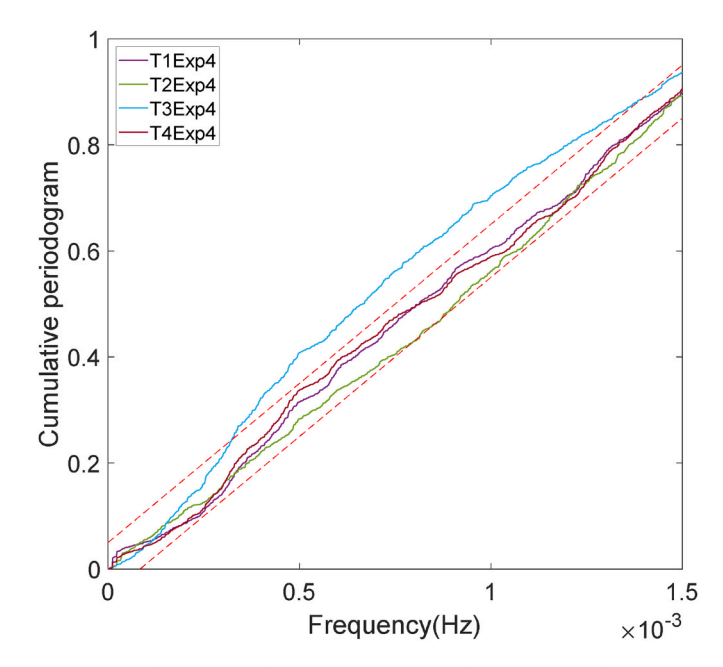


**Fig. 7.** Cumulative periodogram of the residuals of the model 3R2C for different types of indoor temperature measurement.

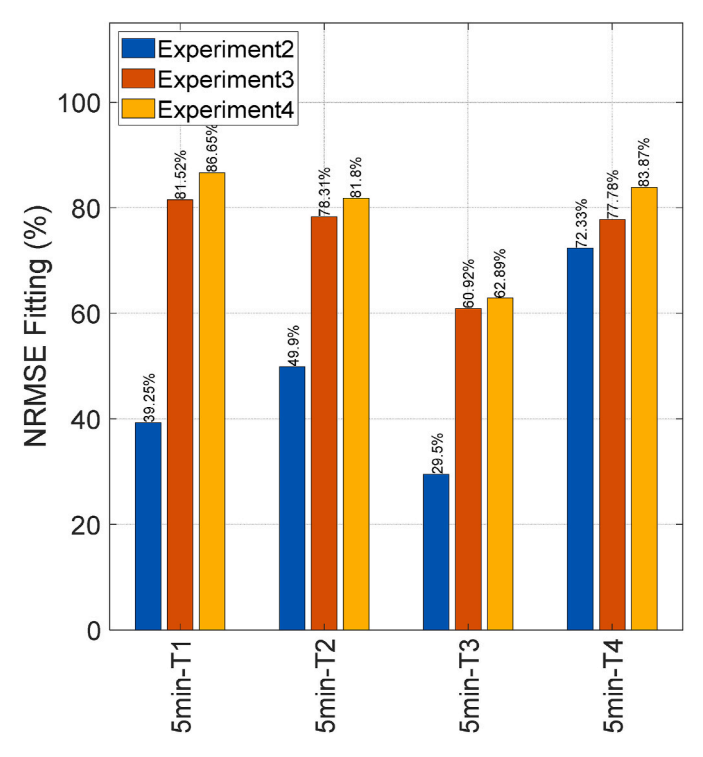


**Fig. 8.** Comparing the one-day ahead prediction of the 3R2C stochastic (sto) models with different types of temperature measurement, trained using Experiment 4 and validated using Experiments 2, 3.

# 4.3.1. Influence of data-preprocessing on the deterministic model

Fig. 9 presents the identified parameters results for the deterministic model using different types of temperature measurement and data preprocessing.

The identified values of HTC show that no matter which type of temperature is used for the identification, the HTC value is not significantly influenced by the pre-filtering method and ACS. The value is close to the reference value of  ${\sim}83$  W/K. The sampling time (Ts) does not have a noticeable impact on the HTC value.

The identified values of  $C_e$  give similar conclusions as the HTC value. The value of  $C_e$  is plausible for most of the cases since it is within the typical range (i.e., 3.4–6.5 kWh/K) given in standards [53]. The low-pass filtering and the ACS only have a slight impact on the results. With direct sampling, the  $C_e$  values are slightly outside the reference range when the sampling time is large (from 30 min). These conclusions are confirmed by the analysis of the effective window area  $A_i$  (related to the influence of solar radiation).

Regarding the simulation performance of the deterministic model, the influence of data pre-processing and the type of temperature measurement are also limited as are the identified parameters. Consequently, the simulation performance is only demonstrated for the volume-averaged temperature (see Fig. 10).

Several main conclusions can be drawn concerning the deterministic model. They are in good agreement with the findings of Yu et al. [26] using virtual experiments. Firstly, the pre-processing of data does not have a considerable influence on the deterministic model. Secondly, the pre-filtering technique could slightly contribute to a more stable estimation of the values if the sampling time  $T_{\mbox{\tiny S}}$  is large (>30 min). Thirdly, the influence of data pre-processing on simulation performance is negligible.

#### 4.3.2. Influence of data-preprocessing on the stochastic model

As shown in Fig. 11, the data pre-processing has a more substantial influence on the identified HTC value for the stochastic model. The ACS can contribute to preventing the HTC value from becoming non-physical

(stays close to the target reference value) for large sampling times. If the filter and the ACS are applied together, the identified HTC value remains stable and close to the reference value for the stochastic model. However, the identified HTC values are often non-physical using the baseline 3R2C model when the dynamics of the wall-mounted temperature sensors are not modeled, even when the sampling time becomes large. Again, only the adapted 3R2C model with a sensor node gives plausible HTC values. This result is counterintuitive. In Section 4.2, the time constant of the wall-mounted sensor has been estimated to be about 8 min. Therefore, it could be expected that the effect of the sensor dynamics would be filtered out by taking a larger sampling time (>15 min). However, this is not the case. This last conclusion is much clearer when analyzing  $C_{\rm e}$ .

The identified C<sub>e</sub> for the stochastic model without and with ACS are shown in Fig. 11, respectively. This confirms the positive effect of ACS for large sampling times. For cases without ACS, the identified C<sub>e</sub> value and variance become non-physical when the sampling time is larger. The C<sub>e</sub> values from volume-averaged temperature (T<sub>1</sub>) and the single wireless temperature (T<sub>2</sub>) sensors remain physically plausible for the large sampling times if the filter and ACS are applied simultaneously. Regarding the wall-mounted sensor, the baseline 3R2C model (T<sub>3</sub>) does not give plausible C<sub>e</sub> values even for large sampling times. The low-pass filtering or ACS does not improve the performance. This confirms that, even though the sensor time constant (~8 min) is significantly shorter than the sampling time, its influence is not filtered out and it still impacts the performance of the stochastic model. For the adapted model (T<sub>4</sub>), the C<sub>e</sub> value remains physically plausible for large sampling times when the ACS and the low-pass filter are applied, just like the datasets T<sub>1</sub> and T<sub>2</sub>. It is worth mentioning that the C<sub>e</sub> values from a single sensor are generally larger than those identified from the volume-averaged temperature.

At this stage, the influence of the ACS does not need to be further demonstrated. Therefore, the  $A_i$  values for the stochastic model are only shown in Fig. 11 with ACS. The results for  $A_i$  are consistent with the results for  $C_e$  and confirm the previous conclusions.

The identified  $\tau$  values for the adapted 3R2C model with a sensor node can be found in Table 5. The sampling time  $(T_s)$  of 5 min is shorter than the identified time constant of about 8 min. However, when the  $T_s$  becomes significantly larger than 8 min,  $\tau$  cannot understandably be identified at a lower value than  $T_s$ . In other words, a sound conclusion is that if the identified sensor time constant is to be physically plausible, the data should be sampled at a higher frequency than the sensor dynamics.

Fig. 12 compares the ability of the model to perform MPC using the one-day ahead prediction performance for the stochastic model identified using the volume-averaged temperature ( $T_1$ ). Large sampling times have a limited effect on the one-day ahead prediction performance. The low-pass filter increases the one-day ahead prediction mainly for the validation datasets using Experiment 2. While the ACS improves the physical plausibility of the model parameters for large sampling times, its influence on the one-day ahead prediction performance is not systematic: it has a slightly positive impact on Experiments 3 and 4 but a negative influence on Experiment 2.

For the case of wall-mounted temperature sensors, the improvement from the adapted model for the one-day ahead prediction performance is significant. The results are shown in Fig. 13 and Fig. 14. If the same preprocessing is applied (i.e., sampling time and filtering method), the NRMSE fitting from the adapted 3R2C stochastic model with sensor node ( $T_4$ ) is always higher than the baseline 3R2C stochastic model without sensor node ( $T_3$ ). Using the wall-mounted sensor, the influence of large sampling time is considerable. However, this effect is reduced using low-pass filtering. The influence of ACS is still not systematic. Nevertheless, for the adapted model, the ACS systematically improves the prediction performance.

To sum up, except for wall-mounted sensors, large  $T_s$  have a limited effect on the prediction performance, which is in good agreement with

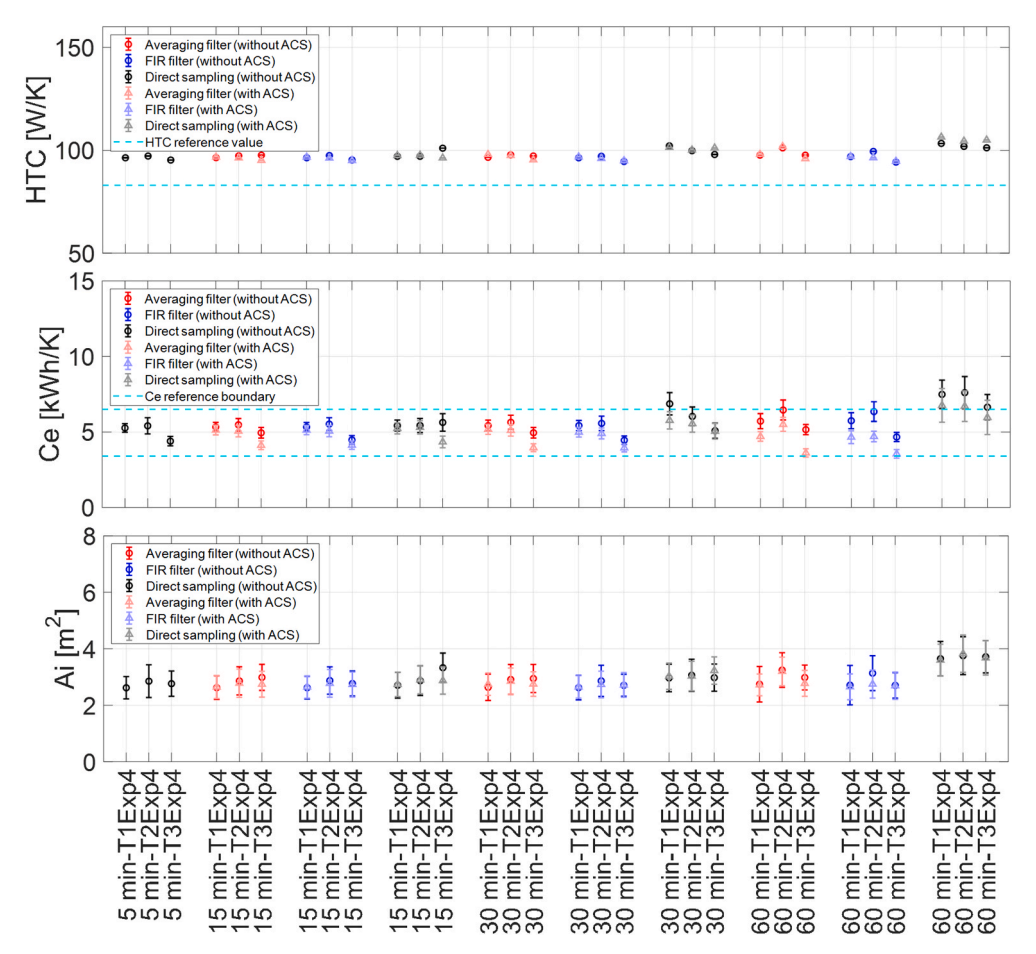


Fig. 9. Identified HTC, Ce and Ai of the 3R2C deterministic model for Experiment 4 with different types of temperature, data pre-processing techniques.

the findings of Yu et al. [26]. For the wall-mounted sensor, additional measures should be taken to conserve the prediction performance with large  $T_s$ . As for the physical plausibility, the low-pass filtering improves the prediction performance. However, the positive influence of the ACS for  $T_s$  is not as systematic for the prediction performance as it was for the

physical plausibility of the parameters.

## 4.3.3. Stochastic model with hydronic radiator

As previously mentioned, the air temperature was only measured using the wall-mounted sensors for the experiment using the hydronic

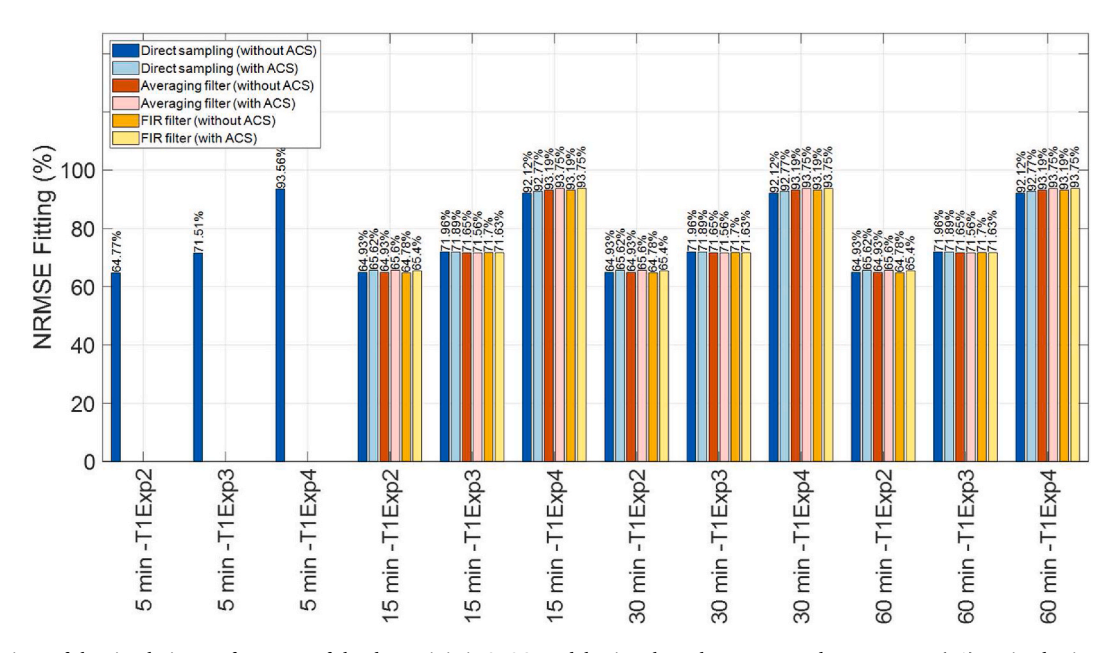


Fig. 10. Comparison of the simulation performance of the deterministic 3R2C model using the volume-averaged temperature (T1), trained using Experiment 4 and validated using Experiments 2, 3.

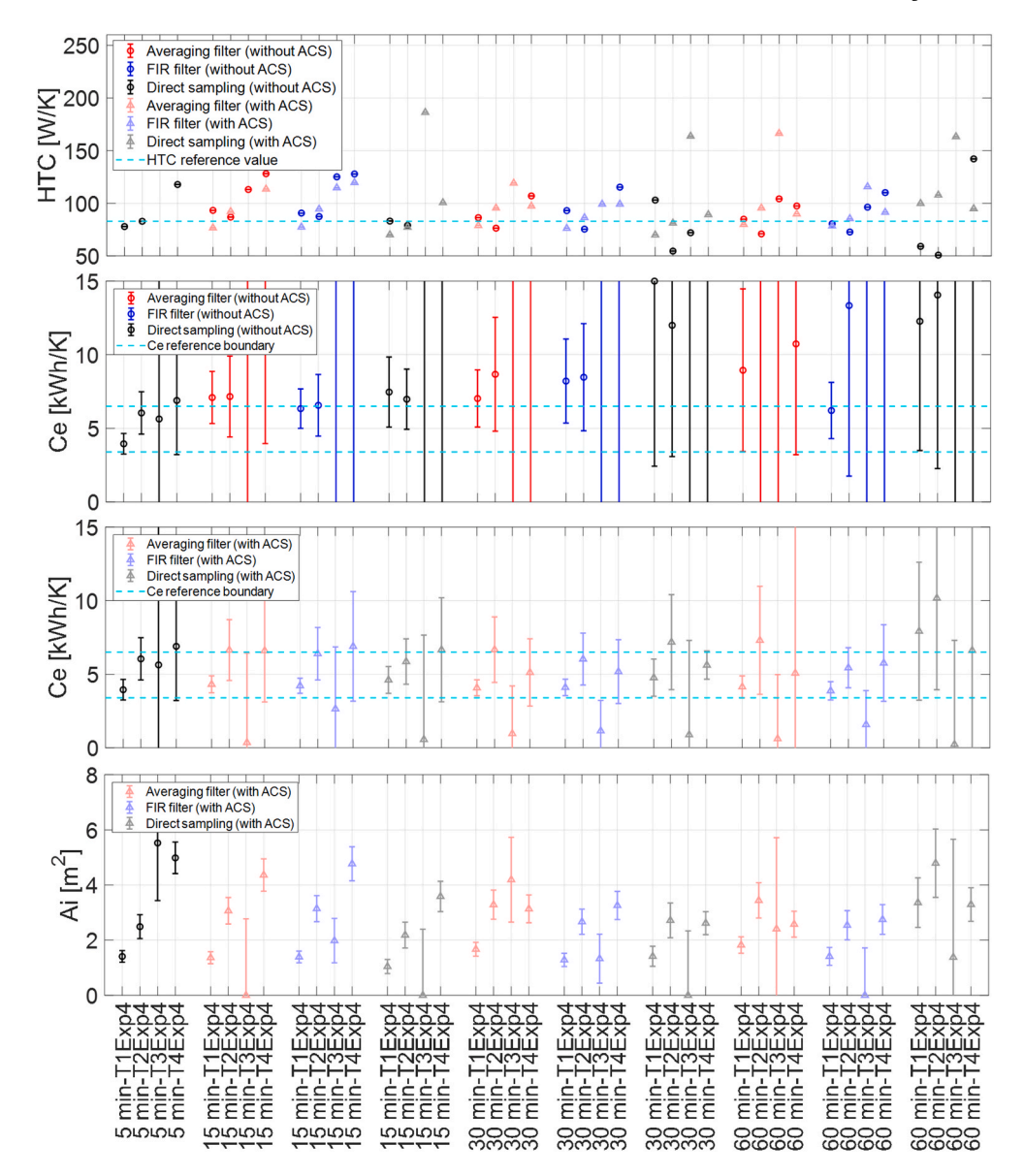


Fig. 11. Identified HTC, Ce and Ai of the 3R2C stochastic model for Experiment 4 with different types of temperature measurement and data pre-processing techniques.

radiator. As it has been proven that the sensor node was necessary for the modeling, only the performance of the adapted model is analyzed. Unlike the electric heater, the thermal dynamics of the hydronic radiator are significant (see Section 2.4). The analysis of the measured inlet and outlet temperatures of the hydronic radiator showed that its time

**Table 5** Identified time constant  $(\tau)$  of the 3R2C adapted stochastic model for Experiment 4 with different data pre-processing techniques.

Sampling	DS		MA		FIR		
time [min]	τ value [min]	τ variance [min]	τ value [min]	τ variance [min]	τ value [min]	τ variance [min]	
5	8.28	0.420	-	_	-	_	
15	16.4	1.82	12.9	1.21	11.6	1.04	
30	67.9	62.1	26.2	3.59	27.6	4.08	
60	97.6	19,465	79.1	1031	76.5	223	

constant is about 7 min. A priori, like the wall-sensor, it is expected that the hydronic radiator dynamics should influence the model performance, at least for a sampling time of 5 min (<7 min). However, the wall-mounted temperature sensor has a time constant of about 8 min. Consequently, the dynamics of the hydronic radiator cannot be properly captured by a grey-box model since the time constant of the wall-mounted sensor is comparable (or slightly larger) than the time constant of the hydronic radiator. The analysis of the cumulative periodogram (not reported here for the sake of the conciseness) shows that the adapted 3R2C can model the building heated using the hydronic radiator without the need to add a specific capacitance to model the hydronic radiator. In addition, preliminary results with an additional capacitance proved that the resulting model would be overfitted.

The experiments with the hydronic radiator and the electric heater have been performed in different years and different months of the heating season, leading to different sun elevations between the experiments. The identified effective window area  $A_i$  is thus expected to be significantly different for Experiment 5 and Experiments 2 to 4. Thermal properties that are intrinsic to the building fabric and less dependent on

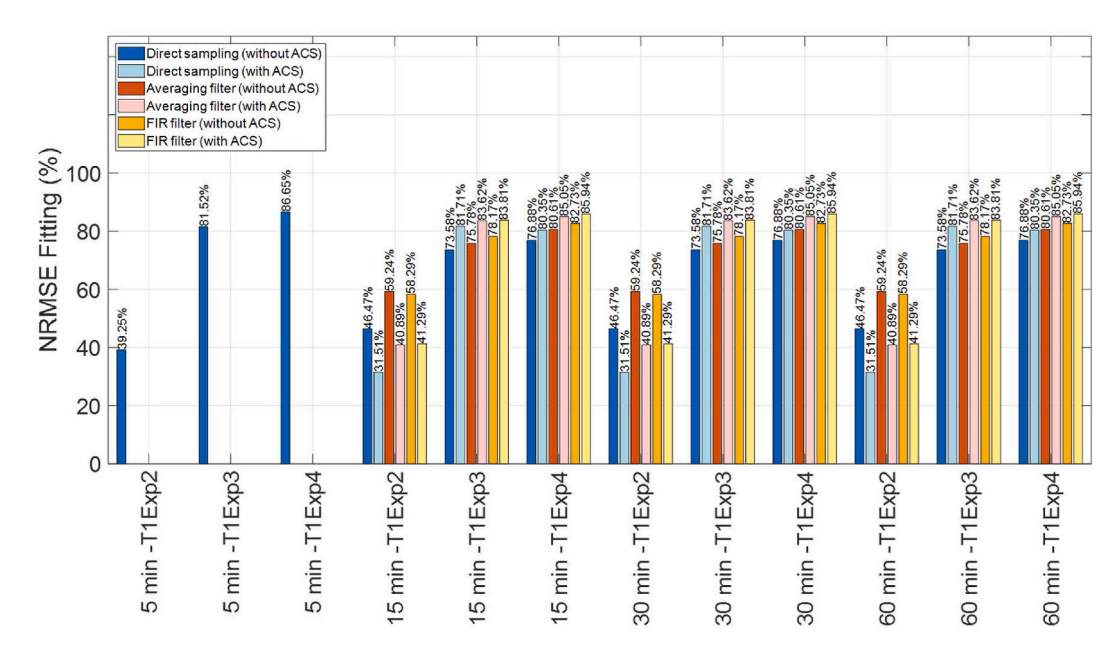


Fig. 12. One-day ahead prediction of the stochastic 3R2C model using the volume-averaged temperature (T1), trained using Experiment 4 and validated using Experiments 2, 3.

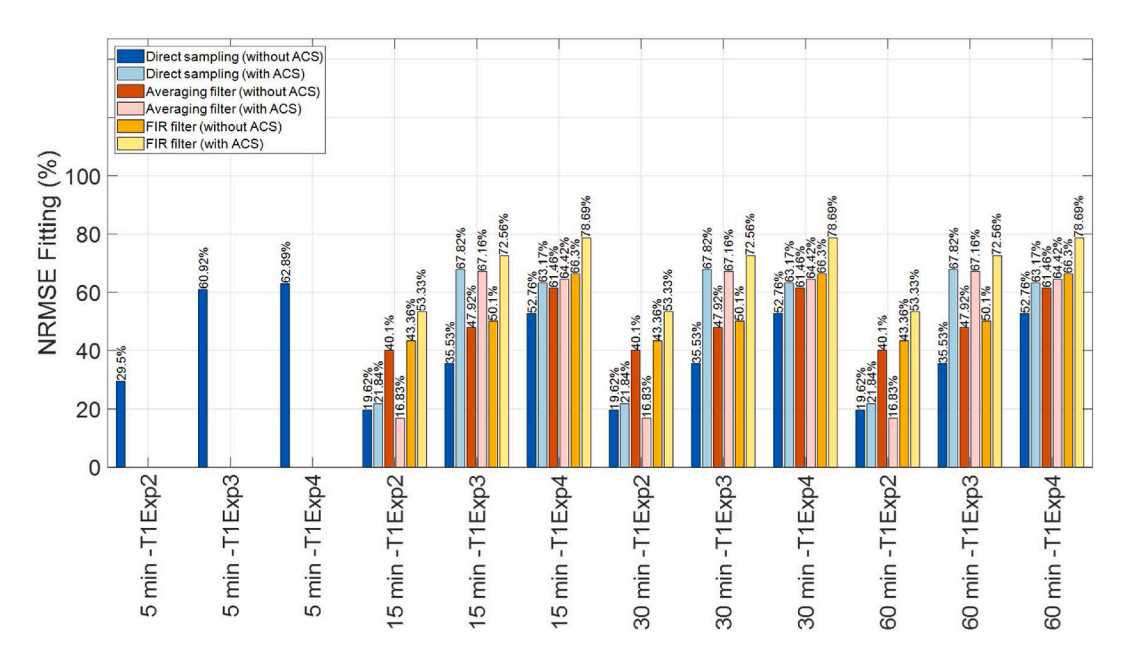


Fig. 13. One-day ahead prediction of the baseline stochastic 3R2C model using a single wall-mounted sensor (T3), trained using Experiment 4 and validated using Experiments 2, 3.

the outdoor conditions are used to analyze the model performance in Experiment 5, namely the HTC and  $C_e$  (Fig. 15). The identified HTC is still close to the reference value. Unlike the experiments with the electric heater, there is no significant difference between the baseline and adapted 3R2C models and the HTC remains plausible for large sampling times (with ACS)

However, the improvement resulting from the adapted model and ACS is more visible when analyzing  $C_{\rm e}$ . Again, the HTC translates into a steady-state performance while the capacitances are inherently related to the building dynamics. Conclusions with the hydronic radiator are in line with the conclusions using Experiment 4 with the electric heater. With the baseline 3R2C model, the estimated  $C_{\rm e}$  is entirely non-physical even using pre-filtering and ACS. The results are noticeably improved with the adapted 3R2C model with a sensor node. If the pre-filtering and

ACS are applied, the  $C_e$  value strictly stays within the reference range no matter how large the sampling time is. For Experiment 5, it is worth mentioning that the quality of the adapted 3R2C model is marginal as the variance  $C_e$  is sometimes very large. Nevertheless, this does not impact the main conclusion. The experiment with the hydronic radiator confirms the positive influence of the adapted model with  $\tau$ , the low-pass filtering and the ACS for large sampling times.

#### 5. Discussion

This paper analyzes the influence of data pre-processing and sensor dynamics on the grey-box modeling of the building thermal dynamics using the MATLAB system identification toolbox. Some limitations to the work can be listed and discussed:

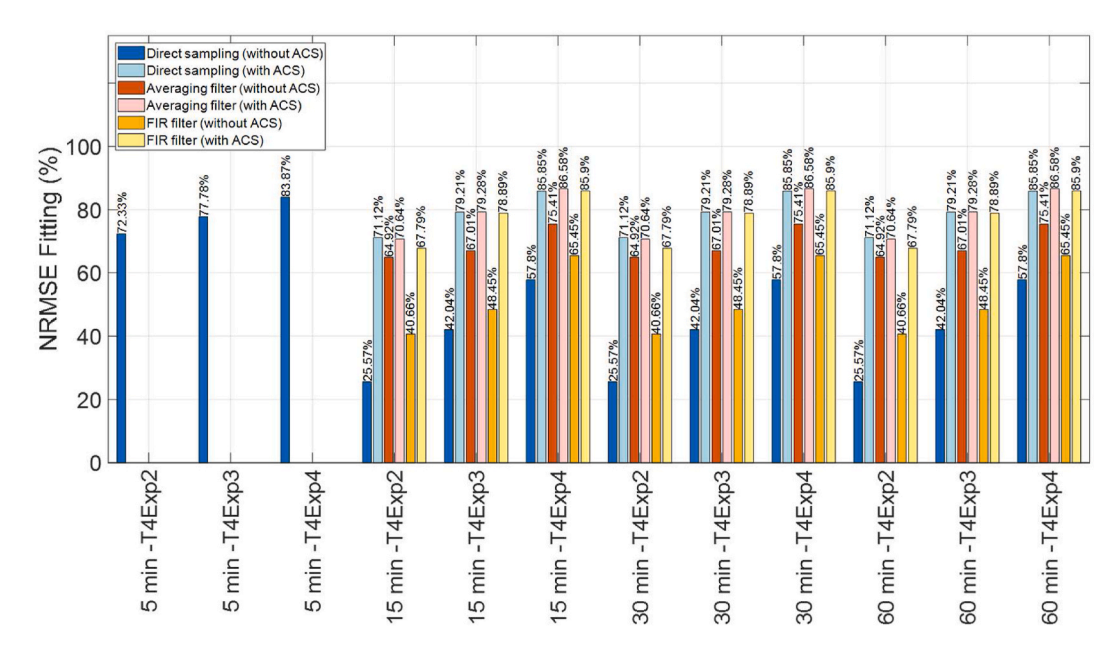
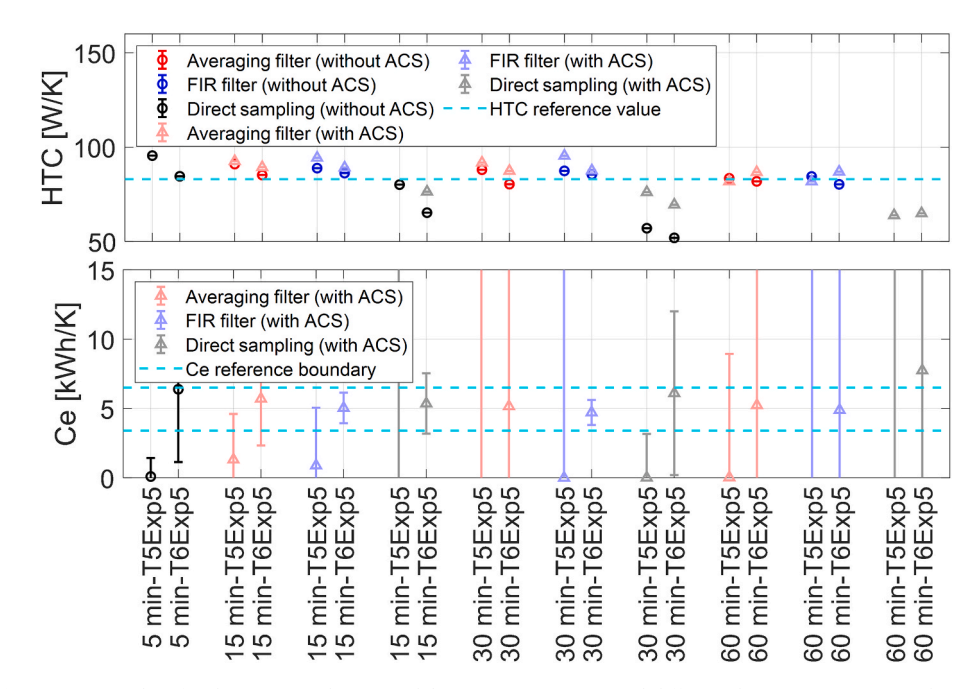


Fig. 14. One-day ahead prediction of the adapted stochastic 3R2C model using a single wall-mounted sensor (T4), trained using Experiment 4 and validated using Experiments 2, 3.



 $\textbf{Fig. 15.} \ \ \textbf{HTC} \ \ \textbf{and} \ \ C_e \ \ \textbf{for the 3R2C} \ \ \textbf{stochastic model using Experiment 5} \ \ \textbf{and different data pre-processing techniques}.$ 

- Important conclusions based on virtual experiments have already been drawn in the previous study of Yu et al. [26]. However, field measurements are different from virtual experiments. The paper succeeded in extending the conclusions from virtual experiments to a real test case with field measurements. However, more test cases are needed to have a generalization of the conclusions. It has been decided to limit the paper to a single test case. The experimental setup and the methodology should be sufficiently described to make the results transparent and reproducible. For the sake of conciseness, this limits the paper to a single test case.
- The test case is a super-insulated building with balanced mechanical ventilation and an energy-efficient heat recovery unit. This enabled the building to be modeled as a single thermal zone. This test case is
- relatively specific as most of the existing houses in the Norwegian building stock do not have these thermal properties. However, it is expected that the conclusions of the paper regarding data pretreatment are not affected by the insulation level and type of ventilation.
- The paper considers that the data pre-treatment is performed equally for all input and output data. This is possible when the data pre-treatment is performed explicitly by the modeler. However, when the data pre-treatment is performed implicitly by the hardware (i.e., the sensor or the DAQ), this pre-treatment can affect the input and output data differently. In this case, additional data pre-treatment techniques should be considered (such as the identification of lag). The conclusions of the paper need to be extended to this case as well.

 The analysis is based on the MATLAB system identification toolbox, where the stochastic equations are written in innovation form. For the generalization, results should be reproduced in other system identification tools and formulations, such as CTSM-R [54].

#### 6. Conclusion

This study is based on two experimental setups using two different space-heating emission systems, namely an electric heater and a hydronic radiator. The pre-processing techniques include low-pass filtering (using MA or FIR), the sampling time ( $T_{\rm S}$ ) and the application of anticausal shift (ACS). Three different types of temperature measurements are analyzed to investigate the influence of the sensor selection and dynamics (i.e. volume-averaged air temperature, single temperature sensor without casing and single wall-mounted sensor).

To analyze the specific influence of the data pre-processing, it is important to ensure that the model performance is not polluted by other phenomena, such as overfitting or poor model fidelity. Therefore, the study starts by selecting a suitable structure for the grey-box model and proves that a mono-zone second-order model is an appropriate trade-off, with (1) a good prediction performance and (2) good interpretability of the physical parameters of the model (i.e., physical plausibility) (3) without beginning to be overfitted. Consequently, a mono-zone 3R2C model is taken as the baseline structure to illustrate the key research questions of the paper. Conclusions are presented separately between deterministic and stochastic models.

Deterministic model:

Yu et al. [26] used virtual experiments and the data pre-processing
has a limited influence on the model performance. This is
confirmed using field experiments. In addition, the sensor thermal
dynamics also has a limited influence on the deterministic model
performance.

Stochastic model:

- Yu et al. [26] used virtual experiments and the parameters became non-physical without ACS for large sampling time (T<sub>s</sub>). On the contrary, large sampling times did not alter the simulation performance significantly. Although the ACS tends to improve the physical plausibility of the model parameters with T<sub>s</sub>, in general, it had a negative influence on the simulation performance of the model.
- These results are partly confirmed using field measurements. Like in Yu et al. [26], large T<sub>s</sub> can cause the parameters to become non-physical without ACS. ACS is excessively beneficial to guarantee the physical plausibility of parameters, making the identified parameters insensitive to the sampling time. Like in Yu et al. [26], large T<sub>s</sub> has a limited effect on the prediction performance for the temperature sensors without casing. However, for the wall-mounted sensor, pre-filtering and sometimes ACS should be used to converse the prediction performance at large T<sub>s</sub>. Like Yu et al. [26] pre-filtering has a beneficial influence on the model performance but not in a dominant way. Unlike Yu et al. [26], the influence of ACS on

- prediction performance is most often beneficial in our study. At this stage, it can be concluded that the influence of the sampling time and ACS on the prediction performance is not systematic (i.e., sometimes positive or negative).
- The results for stochastic models depend on the type of temperature measurement. Firstly, the cases with temperature sensors with negligible thermal dynamics (i.e., free-standing air temperature sensor without casing) are analyzed. Even though the vertical thermal stratification is significant, there is only a slight reduction in the model performance when moving from a volume-averaged measurement to a single sensor located at mid-height in the room. Secondly, when the temperature sensor is the wall-mounted temperature sensor, an adapted model with time constant dynamics for the sensor is needed to obtain a physically plausible estimation of the parameters. This is an important conclusion as most buildings are equipped with wall-mounted temperature sensors. To limit the investment, the number of sensors should also be limited, making a volume-averaged measurement expensive.
- The dynamics of the hydronic radiator (with significant thermal mass) are not necessary to be modeled if the time constant of the measurement device is larger than that of the hydronic radiator.

As the article is based on a single test case, additional research on real buildings is needed to generalize the conclusions. These findings provide practical guidelines to identify the thermal dynamics of buildings using grey-box models and field measurement data.

# CRediT authorship contribution statement

Xingji Yu: Conceptualization, Data curation, Formal analysis, Investigation, Methodology, Software, Validation, Visualization, Writing – original draft. Kristian Stenerud Skeie: Data curation, Writing – review & editing. Michael Dahl Knudsen: Writing – review & editing, Investigation. Zhengru Ren: Writing – review & editing, Validation. Lars Imsland: Conceptualization, Methodology, Supervision, Writing – review & editing. Laurent Georges: Writing – review & editing, Validation, Supervision, Methodology, Investigation, Funding acquisition.

#### **Declaration of competing interest**

The authors declare that they have no known competing financial interests or personal relationships that could have appeared to influence the work reported in this paper.

## Acknowledgments

This work is conducted in the framework of the Norwegian Research Centre on Zero Emission Neighbourhoods in Smart Cities (ZEN), cofunded by the Research Council of Norway and industry partners. In addition, this research is also a contribution to IEA EBC Annex 81 on Data-Driven Smart Buildings.

# Appendix A. Supplementary data

Supplementary data to this article can be found online at https://doi.org/10.1016/j.buildenv.2022.108832.

#### Appendix

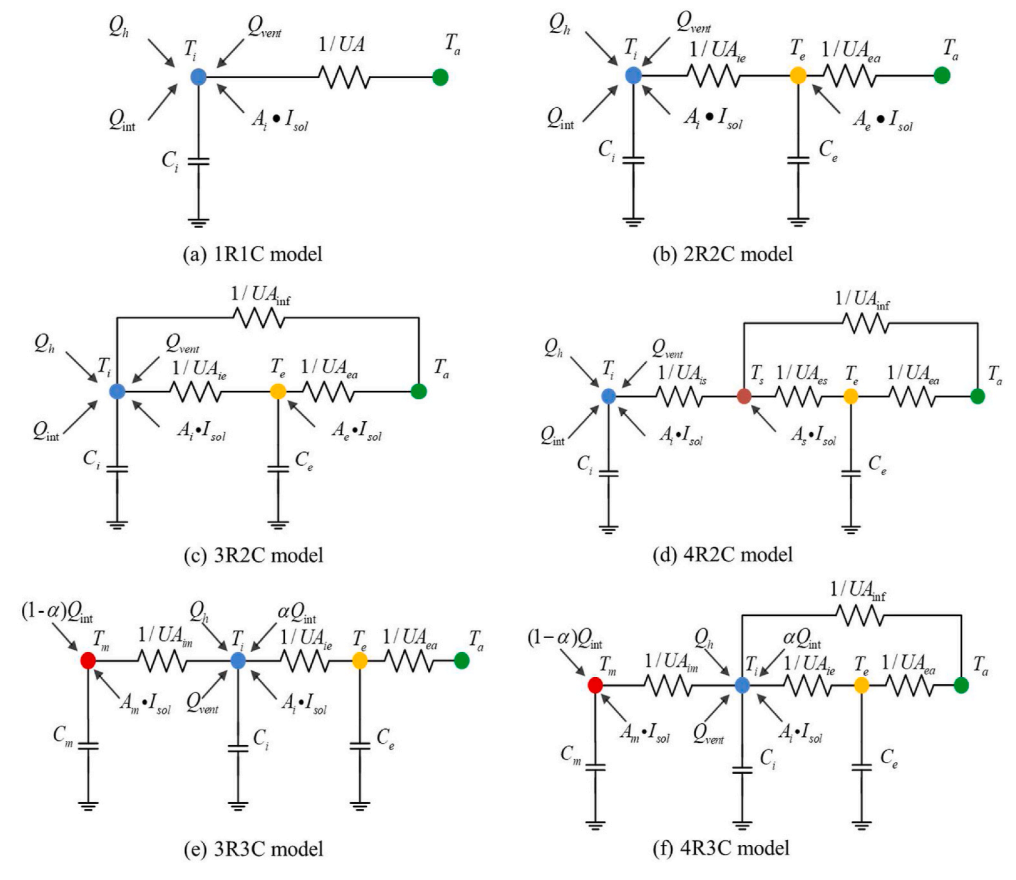


Fig. 16. Grey-box model structures except for the most complicated 5R3C model.

Table 6
Model identification results of the candidate models with 5 min data and volume-averaged temperature (T1), values highlighted with bold color are non-physical values.

Model	UA <sub>ea</sub> [W/K]	UA <sub>ie</sub> [W/K]	$UA_{im}[W/K]$	$UA_{inf}\left[W/K\right]$	UA [W/K]	UA <sub>as</sub> [W/K]	UA <sub>es</sub> [W/K]	UA <sub>is</sub> [W/K]	C <sub>e</sub> [kWh/K]	C <sub>i</sub> [kWh/K]
1R1Cdet	_	_	_	_	106	_	_	_	-	5.62
2R2Cdet	114	826	_	_	_	_	_	_	6.11	0.749
3R2Cdet	80.2	876	-	23.0	_	-	-	_	5.28	0.767
4R2Cdet	52.1	_	-	51.5	_	-	2558	1345	5.40	0.781
3R3Cdet	153	404	565	_	_	_	_	_	6.08	0.961
4R3Cdet	104	303	687	26.5	_	_	_	_	3.94	0.909
5R3Cdet	102		686	_	_	28.1	331	4694	3.99	0.908
1R1Csto	_	_	_	_	109	_	_	_	_	4.78
2R2Csto	109	1058	_	_	_	_	_	_	6.37	1.24
3R2Csto	17.1	868	_	63.5	_	_	_	_	4.22	1.15
4R2Csto	0.000	1181	_	78.5	_	_	_	3342	4.28	1.11
3R3Csto	123	552	763	_	_	_	_	_	11.9	1.23
4R3Csto	5.40	692	346	71.4	_	_	_	_	4.02	1.21
5R3Csto	0.000	_	375	-	-	108	8492	1087	5.73	1.19
Model	C <sub>m</sub> [kWh/K]	A <sub>i</sub> [m <sup>2</sup> ]	A <sub>e</sub> [m <sup>2</sup> ]	A <sub>m</sub> [m <sup>2</sup> ]	$A_s$ [ $m^2$ ]	alpha [–]	MBE	NRMSE (one- step)	NRMSE (prediction)	HTC [W/K]
1R1Cdet	_	2.99	_	_	-	_	0.0010	_	72.7%	105
2R2Cdet	_	2.96	0.000	_	_	_	0.0007	_	93.0%	100
3R2Cdet	_	2.62	0.000	_	_	_	0.0008	_	93.6%	96.4
4R2Cdet	_	2.78	_	_	0.000	_	-0.0033	_	93.5%	103
3R3Cdet	2.09	3.82	_	0.000	_	0.500	-0.0017	_	95.0%	111
3R3Cdet 4R3Cdet	2.09 2.58	3.82 3.19		0.000 0.000	_	0.500 0.500	-0.0017 $0.0025$	_	95.0% 95.3%	111 104
					- - 3.21					
4R3Cdet	2.58	3.19	-	0.000	-	0.500	0.0025		95.3%	104
4R3Cdet 5R3Cdet	2.58	3.19	-	0.000 0.000	- 3.21	0.500 0.500	$0.0025 \\ -0.0017$	-	95.3% 95.3%	104 106
4R3Cdet 5R3Cdet 1R1Csto	2.58 2.54	3.19 - 3.39	- - -	0.000 0.000 -	- 3.21 -	0.500 0.500 -	$0.0025 \\ -0.0017 \\ -0.0008$	- - 99.0%	95.3% 95.3% 73.4%	104 106 109
4R3Cdet 5R3Cdet 1R1Csto 2R2Csto	2.58 2.54 -	3.19 - 3.39 3.07	- - - 0.000	0.000 0.000 - -	- 3.21 - -	0.500 0.500 - -	0.0025 -0.0017 -0.0008 0.0000	- - 99.0% 99.2%	95.3% 95.3% 73.4% 87.3%	104 106 109 98.8
4R3Cdet 5R3Cdet 1R1Csto 2R2Csto 3R2Csto	2.58 2.54 -	3.19 - 3.39 3.07 1.56	- - 0.000 0.122	0.000 0.000 - -	- 3.21 - -	0.500 0.500 - -	0.0025 -0.0017 -0.0008 0.0000 0.0000	- 99.0% 99.2% 99.2%	95.3% 95.3% 73.4% 87.3% 87.2%	104 106 109 98.8 80.3
4R3Cdet 5R3Cdet 1R1Csto 2R2Csto 3R2Csto 4R2Csto	2.58 2.54 - - -	3.19 - 3.39 3.07 1.56 1.09	- - 0.000 0.122	0.000 0.000 - - -	- 3.21 - - - 0.686	0.500 0.500 - - -	0.0025 -0.0017 -0.0008 0.0000 0.0000 0.0001	- 99.0% 99.2% 99.2% 99.2%	95.3% 95.3% 73.4% 87.3% 87.2% 86.6%	104 106 109 98.8 80.3 78.5

#### References

- [1] J. Drgoňa, J. Arroyo, I. Cupeiro Figueroa, D. Blum, K. Arendt, D. Kim, E.P. Ollé, J. Oravec, M. Wetter, D.L. Vrabie, L. Helsen, All you need to know about model predictive control for buildings, Annu. Rev. Control 50 (2020) 190–232, https://doi.org/10.1016/j.arcontrol.2020.09.001.
- [2] A.E. Ruano, E.M. Crispim, E.Z.E. Conceição, M.M.J.R. Lúcio, Prediction of building's temperature using neural networks models, Energy Build. 38 (2006) 682–694, https://doi.org/10.1016/j.enbuild.2005.09.007.
- [3] J.A. Crabb, N. Murdoch, J.M. Penman, A simplified thermal response model, Build. Serv. Eng. Technol. 8 (1987) 13–19.
- [4] L. Laret, Use of general models with a small number of parameters, Part 1: theoretical analysis, in: Proc. Conf. Clima, 2000, pp. 263–276.
- [5] A. Afram, F. Janabi-Sharifi, Review of modeling methods for HVAC systems, Appl. Therm. Eng. 67 (2014) 507–519, https://doi.org/10.1016/j. applthermaleng.2014.03.055.
- [6] Y. Li, Z. O'Neill, L. Zhang, J. Chen, P. Im, J. DeGraw, Grey-box modeling and application for building energy simulations - a critical review, Renew. Sustain. Energy Rev. 146 (2021) 111174, https://doi.org/10.1016/j.rser.2021.111174.
- [7] Y. Yao, D.K. Shekhar, State of the art review on model predictive control (MPC) in Heating Ventilation and Air-conditioning (HVAC) field, Build. Environ. 200 (2021) 107952, https://doi.org/10.1016/j.buildenv.2021.107952.
- [8] H. Madsen, P. Bacher, G. Bauwens, A.-H. Deconinck, G. Reynders, S. Roels, E. Himpe, G. Lethé, IEA EBC Annex 58-Reliable Building Energy Performance Characterisation Based on Full Scale Dynamic Measurements, Report of subtask 3, part 2: thermal performance characterisation using time series data-statistical guidelines, 2016, https://www.iea-ebc.org/Data/publications/EBC\_Annex\_58\_Fi nal Report ST3b.pdf.
- [9] S. Stinner, K. Huchtemann, D. Müller, Quantifying the operational flexibility of building energy systems with thermal energy storages, Appl. Energy 181 (2016) 140–154, https://doi.org/10.1016/j.apenergy.2016.08.055.
- [10] N.G. Paterakis, O. Erdinç, J.P.S. Catalão, An overview of Demand Response: keyelements and international experience, Renew. Sustain. Energy Rev. 69 (2017) 871–891, https://doi.org/10.1016/j.rser.2016.11.167.
- [11] G. Steindl, W. Kastner, V. Stangl, Comparison of data-driven thermal building models for model predictive control, J. Sustain. Dev. Energy, Water Environ. Syst. 7 (2019) 730–742, https://doi.org/10.13044/j.sdewes.d7.0286.
- [12] P. Siano, Demand response and smart grids a survey, Renew. Sustain. Energy Rev. 30 (2014) 461–478, https://doi.org/10.1016/j.rser.2013.10.022.
- [13] M. Dahl Knudsen, S. Petersen, Demand response potential of model predictive control of space heating based on price and carbon dioxide intensity signals, Energy Build. 125 (2016) 196–204, https://doi.org/10.1016/j. ephuild.2016.04.053.
- [14] S.Ø. Jensen, A. Marszal-Pomianowska, R. Lollini, W. Pasut, A. Knotzer, P. Engelmann, A. Stafford, G. Reynders, IEA EBC Annex 67 energy flexible buildings, Energy Build. 155 (2017) 25–34, https://doi.org/10.1016/j. ephylid/2017.08.044
- [15] M. Killian, M. Kozek, Ten questions concerning model predictive control for energy efficient buildings, Build. Environ. 105 (2016) 403–412, https://doi.org/10.1016/ i.buildenv.2016.05.034.
- [16] H. Harb, N. Boyanov, L. Hernandez, R. Streblow, D. Müller, Development and validation of grey-box models for forecasting the thermal response of occupied buildings, Energy Build. 117 (2016) 199–207, https://doi.org/10.1016/j. enbuild.2016.02.021.
- [17] J. Le Dréau, P. Heiselberg, Energy flexibility of residential buildings using short term heat storage in the thermal mass, Energy 111 (2016) 991–1002, https://doi. org/10.1016/j.energy.2016.05.076.
- [18] R.E. Hedegaard, T.H. Pedersen, M.D. Knudsen, S. Petersen, Towards practical model predictive control of residential space heating: eliminating the need for weather measurements, Energy Build. 170 (2018) 206–216, https://doi.org/ 10.1016/j.enbuild.2018.04.014.
- [19] S. Freund, G. Schmitz, Implementation of model predictive control in a large-sized, low-energy office building, Build. Environ. 197 (2021) 107830, https://doi.org/ 10.1016/j.buildenv.2021.107830.
- [20] J. Wang, S. Li, H. Chen, Y. Yuan, Y. Huang, Data-driven model predictive control for building climate control: three case studies on different buildings, Build. Environ. 160 (2019) 106204, https://doi.org/10.1016/j.buildenv.2019.106204.
- [21] R. Halvgaard, N.K. Poulsen, H. Madsen, J.B. Jørgensen, Economic model predictive control for building climate control in a smart grid, in: 2012 IEEE PES Innov. Smart Grid Technol., IEEE, 2012, pp. 1–6.
- [22] M.D. Knudsen, R.E. Hedegaard, T.H. Pedersen, S. Petersen, System identification of thermal building models for demand response - a practical approach, Energy Proc. 122 (2017) 937–942, https://doi.org/10.1016/j.egypro.2017.07.426.
- [23] M.A.A. Awadelrahman, Y. Zong, H. Li, C. Agert, Economic model predictive control for hot water based heating systems in smart buildings, Energy Power Eng. 9 (2017) 112–119.
- [24] J.F. van Impe, P.A. Vanrolleghem, D.M. Iserentant, Advanced Instrumentation, Data Interpretation, and Control of Biotechnological Processes, Springer Science & Business Media. 2013.
- [25] L. Ljung, A. Wills, Issues in sampling and estimating continuous-time models with stochastic disturbances, Automatica 46 (2010) 925–931, https://doi.org/10.1016/ j.automatica.2010.02.011.
- [26] X. Yu, L. Georges, L. Imsland, Data pre-processing and optimization techniques for stochastic and deterministic low-order grey-box models of residential buildings,

- Energy Build. 236 (2021) 110775, https://doi.org/10.1016/j.enbuild.2021.110775.
- [27] T. Kalamees, IDA ICE: the simulation tool for making the whole building energy and HAM analysis, Annex 41 (2004) 12–14.
- [28] P. Vogler-Finck, J. Clauß, L. Georges, A dataset to support dynamical modelling of the thermal dynamics of a super-insulated building. https://doi.org/10. 5281/ZENODO.1034820, 2017.
- [29] M.D. Knudsen, L. Georges, K.S. Skeie, S. Petersen, Experimental test of a black-box economic model predictive control for residential space heating, Appl. Energy 298 (2021) 117227, https://doi.org/10.1016/j.apenergy.2021.117227.
- [30] G. Bellu, M.P. Saccomani, S. Audoly, L. D'Angiò, DAISY: a new software tool to test global identifiability of biological and physiological systems, Comput. Methods Progr. Biomed. 88 (2007) 52–61, https://doi.org/10.1016/j.cmpb.2007.07.002.
- [31] M.P. Saccomani, S. Audoly, G. Bellu, L. D'Angiò, Examples of testing global identifiability of biological and biomedical models with the DAISY software, Comput. Biol. Med. 40 (2010) 402–407, https://doi.org/10.1016/j. compbiomed.2010.02.004.
- [32] P.J.C. Vogler-Finck, J. Clauß, L. Georges, I. Sartori, R. Wisniewski, Inverse model identification of the thermal dynamics of a Norwegian zero emission house, in: Cold Clim. HVAC Conf., Springer, 2018, pp. 533–543.
- [33] L. Georges, M.J. Alonso, R. Woods, K. Wen, F. Håheim, P. Liu, M. Berge, M. Thalfeldt, Evaluation of Simplified Space-Heating Hydronic Distribution for Norwegian Passive Houses, SINTEF akademisk forlag, 2017. https://www. sintefbok.no/book/index/1123/evaluation\_of\_simplified\_space-heating\_h ydronic\_distribution\_for\_norwegian\_passive\_houses#carousel.
- [34] X. Yu, L. Georges, M.D. Knudsen, I. Sartori, L. Imsland, Investigation of the model structure for low-order grey-box modelling of residential buildings, in: Proc. Build. Simul. 2019 16th Conf. IBPSA, International Building Performance Simulation Association, IBPSA, 2019, https://doi.org/10.26868/25222708.2019.211209.
- [35] H. Viot, A. Sempey, L. Mora, J.C. Batsale, J. Malvestio, Model predictive control of a thermally activated building system to improve energy management of an experimental building: Part I—modeling and measurements, Energy Build. 172 (2018) 94–103, https://doi.org/10.1016/j.enbuild.2018.04.055.
- [36] P. Bacher, H. Madsen, Identifying suitable models for the heat dynamics of buildings, Energy Build. 43 (2011) 1511–1522, https://doi.org/10.1016/j. enbuild.2011.02.005.
- [37] T. Berthou, P. Stabat, R. Salvazet, D. Marchio, Development and validation of a gray box model to predict thermal behavior of occupied office buildings, Energy Build. 74 (2014) 91–100, https://doi.org/10.1016/j.enbuild.2014.01.038.
- [38] J.E. Braun, N. Chaturvedi, An inverse gray-box model for transient building load prediction, HVAC R Res. 8 (2002) 73–99, https://doi.org/10.1080/ 10789669.2002.10391290.
- [39] J. Hu, P. Karava, A state-space modeling approach and multi-level optimization algorithm for predictive control of multi-zone buildings with mixed-mode cooling, Build. Environ. 80 (2014) 259–273, https://doi.org/10.1016/j. buildenv.2014.05.003.
- [40] S. Goyal, P. Barooah, A method for model-reduction of non-linear thermal dynamics of multi-zone buildings, Energy Build. 47 (2012) 332–340, https://doi. org/10.1016/j.enbuild.2011.12.005.
- [41] E. Palomo Del Barrio, G. Lefebvre, P. Behar, N. Bailly, Using model size reduction techniques for thermal control applications in buildings, Energy Build. 33 (2000) 1–14, https://doi.org/10.1016/S0378-7788(00)00060-8.
- [42] G. Reynders, J. Diriken, D. Saelens, Quality of grey-box models and identified parameters as function of the accuracy of input and observation signals, Energy Build. 82 (2014) 263–274, https://doi.org/10.1016/j.enbuild.2014.07.025.
  [43] O.M. Brastein, D.W.U. Perera, C. Pfeifer, N.O. Skeie, Parameter estimation for grey-
- [43] O.M. Brastein, D.W.U. Perera, C. Pfeifer, N.O. Skeie, Parameter estimation for grey-box models of building thermal behaviour, Energy Build. 169 (2018) 58–68, https://doi.org/10.1016/j.enbuild.2018.03.057.
- [44] German Association of Engineers, Calculation of Transient Thermal Response of Rooms and Buildings E Modelling Of Rooms, 91.140.10(VDI 6007), Beuth Verlag GmbH, Düsseldorf, 2012.
- [45] International Organization for Standardization, Energy Performance of Buildings E Calculation of Energy Use for Space Heating and Cooling (ISO 13790:2008), Geneva. 2008.
- [46] M. Hu, F. Xiao, L. Wang, Investigation of demand response potentials of residential air conditioners in smart grids using grey-box room thermal model, Appl. Energy 207 (2017) 324–335, https://doi.org/10.1016/j.apenergy.2017.05.099.
- [47] A.F. Villaverde, A. Barreiro, A. Papachristodoulou, Structural identifiability of dynamic systems biology models, PLoS Comput. Biol. 12 (2016), e1005153.
- [48] O. Chis, J.R. Banga, E. Balsa-Canto, Methods for checking structural identifiability of nonlinear biosystems: a critical comparison, IFAC (2011), https://doi.org/ 10.3182/20110828-6-IT-1002.00800.
- [49] L. Ljung, System Identification Toolbox TM User's Guide, 2014.
- [50] K.J. Åström, Introduction to Stochastic Control Theory, Courier Corporation, 2012.
- [51] J. Wang, H. Chen, Y. Yuan, Y. Huang, A novel efficient optimization algorithm for parameter estimation of building thermal dynamic models, Build. Environ. 153 (2019) 233–240, https://doi.org/10.1016/j.buildenv.2019.02.006.
- [52] J. Clauß, P. Vogler-Finck, L. Georges, Calibration of a high-resolution dynamic model for detailed investigation of the energy flexibility of a zero emission residential building, in: Cold Clim. HVAC Conf., Springer, 2018, pp. 725–736.
- [53] Standard Norge, NS 3031 Energy Performance of Buildings: Calculation of Energy Needs and Energy Supply, 2016.
- [54] R. Juhl, J.K. Møller, H. Madsen, ctsmr-Continuous Time Stochastic Modeling in R, 2016. ArXiv Prepr, 1606.00242.